



# Age-related loss of gene-to-gene transcriptional coordination among single cells

Orr Levy<sup>1,5</sup>, Guy Amit<sup>1,5</sup>, Dana Vaknin<sup>1</sup>, Tom Snir<sup>1</sup>, Sol Efroni<sup>1</sup>, Peter Castaldi<sup>3,4</sup>, Yang-Yu Liu<sup>1</sup>, Haim Y. Cohen<sup>2</sup> and Amir Bashan<sup>1</sup>✉

A long-standing model holds that stochastic aberrations of transcriptional regulation play a key role in the process of ageing. While transcriptional dysregulation is observed in many cell types in the form of increased cell-to-cell variability, its generality to all cell types remains doubted. Here, we propose a new approach for analysing transcriptional regulation in single-cell RNA sequencing data by focusing on the global coordination between the genes rather than the variability of individual genes or correlations between pairs of genes. Consistently, across very different organisms and cell types, we find a decrease in the gene-to-gene transcriptional coordination in ageing cells. In addition, we find that loss of gene-to-gene transcriptional coordination is associated with high mutational load of a specific, age-related signature and with radiation-induced DNA damage. These observations suggest a general, potentially universal, stochastic attribute of transcriptional dysregulation in ageing.

**D**uring ageing, somatic cells accumulate various types of random damage, including genetic and epigenetic mutations<sup>1,2</sup>. A fundamental question in ageing is how such a stochastic process may eventually lead to ageing phenotypes. Several central theories relate random damage accumulation to specific mechanisms of disruption of particular cellular elements<sup>3</sup>—for example, shortening telomeres<sup>4</sup> and programmed cellular responses such as apoptosis or senescence<sup>5</sup> that accompany age-related decline of proper functioning. In principle, recognizing these mechanisms can guide the rational development of targeted therapeutic interventions<sup>6</sup>. Alternatively, it has been suggested that the decline of tissue function could be also caused without any specifically defined mechanism, merely as a result of a stochastic process of increased transcriptional disorder where stochastic alteration of gene regulatory circuits in different individual cells disrupts the orchestrated gene expression in the tissue<sup>7–11</sup>.

Because such stochasticity affects individual cells in different ways, it cannot be directly captured by bulk analyses, which represents the behaviour of an ‘average cell’<sup>12</sup>. The increasing prevalence of single-cell RNA sequencing (scRNA-seq) data makes it possible to observe and characterize the form of such transcriptional stochastic dysregulation.

Previous studies on ageing cells have proposed that age-related transcriptional dysregulation in the form of cell-to-cell variability may introduce phenotypic variation among cells that could generally become detrimental to normal tissue function<sup>13,14</sup>. Indeed, such increased transcriptional variability was found first in a selected panel of genes in heart cells<sup>13</sup> and, more recently, in the whole transcriptomes of immune cells<sup>15</sup>, human pancreas cells<sup>16</sup> and various murine lung cell types<sup>17</sup>. However, in some cell types this pattern is not found. For example, despite observations of genetic and epigenetic damage in ageing haematopoietic stem cells<sup>18–21</sup> (HSCs), cell-to-cell transcriptional variability is not observed<sup>22</sup>. Thus, in the absence of consistent empirical support, it remains unclear whether transcriptional dysregulation is indeed a general attribute of ageing

and, if so, what are the affected aspects that conceivably contribute to the progressive loss of physiological function.

Since genes are fundamentally linked both by the underlying regulatory mechanisms and by jointly implementing biological functions, it has been proposed to study age-related transcriptional dysregulation by focusing on the transcriptional interrelations between genes, rather than the activity of each gene separately<sup>23,24</sup>. Indeed, decreasing gene coexpression was demonstrated in ageing mice within genetic modules using microarray data<sup>24</sup>. However, such bulk analysis does not represent the transcriptional dysregulation in individual cells. By studying scRNA-seq data, we can both observe the stochastic transcriptional changes at the resolution of single cells and better focus on specific tissues and cell types. Our goal is to determine, by analysing single-cell transcription profiles from young and old organisms, whether transcriptional dysregulation, as manifested in the interrelation between transcriptional levels of different genes, is a characteristic phenomenon in ageing. We also ask whether it is associated with an increased load of cellular damage.

## Results

**Measuring gene-to-gene transcriptional coordination.** Without a priori knowledge of the intricate map of gene-to-gene regulatory interactions, several methods are commonly used to characterize transcriptional interrelations between genes—for example, based on transcriptional coexpression analysis. In principle, analysis of the changes of coexpression networks calculated for single-cell data could be used to identify patterns of transcriptional dysregulation in ageing. However, this ‘bottom-up’ approach has considerable obstacles. First, coexpression networks estimate the direct or indirect correlations between pairs of genes, while an individual gene may be controlled by multiple regulators<sup>25–29</sup>. Second, each coexpression measure is designed to capture a specific feature that is not necessarily optimal for depicting all types of gene-to-gene transcriptional interrelation (for example, Pearson correlations

<sup>1</sup>Department of Physics, Bar-Ilan University, Ramat-Gan, Israel. <sup>2</sup>The Mina and Everard Goodman Faculty of Life Science, Bar-Ilan University, Ramat-Gan, Israel. <sup>3</sup>Channing Division of Network Medicine, Brigham and Women’s Hospital and Harvard Medical School, Boston, MA, USA. <sup>4</sup>Division of Primary Care and General Medicine, Brigham and Women’s Hospital, Boston, MA, USA. <sup>5</sup>These authors contributed equally: Orr Levy, Guy Amit.

✉e-mail: amir.bashan@biu.ac.il

**Table 1 | List of scRNA-seq datasets analysed in this work**

Organism	Tissue	Cell type	Study	No. of cells (young/old)	Ages (young/old)	Sex
<i>Drosophila</i>	Brain	Antero-dorsal olfactory projection neurons	Davie et al. <sup>45</sup>	24/22	1/50 days	20 females and 10 males
<i>Drosophila</i>	Brain	Neurons of the optic lobes	Davie et al. <sup>45</sup>	39/32	1/50 days	20 females and 10 males
<i>Drosophila</i>	Brain	Glial ensheathing cells	Davie et al. <sup>45</sup>	112/116	1/50 days	20 females and 10 males
<i>Drosophila</i>	Brain	Astrocyte-like cells	Davie et al. <sup>45</sup>	66/269	1/50 days	20 females and 10 males
Mouse, DBA/2	HSCs	MPP-HSCs	Kowalczyk et al. <sup>33</sup>	27/16	2/24 months	Females
Mouse, C57BL/6J	HSCs	MPP-HSCs	Young et al. <sup>46</sup>	23/20	2/28 months	Females
Mouse, C57BL/6J	HSCs	MPP-HSCs	Mann et al. <sup>31</sup>	56/21	2-3/20-24 months	Males and females
Mouse, C57BL/6J	HSCs	LT-HSCs	Grover et al. <sup>34</sup>	47/31	2-3/20-25 months	Males and females
Mouse, C57BL/6J	HSCs	ST-HSCs	Mann et al. <sup>31</sup>	29/38	2-3/20-24 months	Males and females
Mouse, C57BL/6J	HSCs	LT-HSCs	Mann et al. <sup>31</sup>	51/42	2-3/20-24 months	Males and females
Mouse, DBA/2	HSCs	ST-HSCs	Kowalczyk et al. <sup>33</sup>	46/45	2/24 months	Females
Mouse, C57BL/6	HSCs	MPP-HSCs	Kowalczyk et al. <sup>33</sup>	76/46	2/24 months	Females
Mouse, DBA/2	HSCs	LT-HSCs	Kowalczyk et al. <sup>33</sup>	44/54	2/24 months	Females
Mouse, C57BL/6	HSCs	LT-HSCs	Kowalczyk et al. <sup>33</sup>	113/199	2/24 months	Females
Mouse, C57BL/6	HSCs	ST-HSCs	Kowalczyk et al. <sup>33</sup>	118/227	2/24 months	Females
Mouse, C57BL/6J (B6)	Immune	CD4 <sup>+</sup> T cells, stimulated effector memory cells	Martinez et al. <sup>15</sup>	26/29	3/21 months	Males
Mouse, C57BL/6J (B6)	Immune	Stimulated naïve cells	Martinez et al. <sup>15</sup>	30/36	3/21 months	Males
Mouse, C57BL/6J (B6)	Immune	Unstimulated effector memory cells	Martinez et al. <sup>15</sup>	109/115	3/21 months	Males
Mouse, C57BL/6J (B6)	Immune	Unstimulated naïve cells	Martinez et al. <sup>15</sup>	90/121	3/21 months	Males
Human	Pancreas	Glucagon cells	Enge et al. <sup>16</sup>	157/133/226/141/171	21/22/38/44/54 years	Males and females
Cell lines KYSE180	Oesophageal squamous cell carcinoma	Yang et al. <sup>35</sup>	41/88/89	Radiation levels (Gy): 0/12/30	Males and females	

All the datasets analysed in this work have been published. The original experiments and corresponding power analysis have been reported in previous publications. The scRNA-seq data of HSCs of mice are from refs. <sup>33,34,46</sup>, where young and old mice are 2–3 and 20–25 months old from ref. <sup>34</sup>, 2 and 24 months old from ref. <sup>33</sup> and 2 and 28 months old from ref. <sup>46</sup>. The scRNA-seq data of immune cells of mice are from ref. <sup>15</sup> with ages of 3 and 21 months. For neurons and glia cells, the *Drosophila* data are from ref. <sup>45</sup>, where ages of young and old cells are 1 and 50 days. The human pancreatic cell data are from ref. <sup>16</sup>.

represent linear relationships). Third, large calculated coexpression matrices contain a considerable amount of noise, which raises an additional difficulty in exploring their differentiation across cohorts (see further discussion in Supplementary Information and systematic comparison of correlation matrices calculated from cells of young and old organisms in Supplementary Information and Supplementary Fig. 1).

To overcome these obstacles, we propose a ‘top-down’ computational method to evaluate the system-wide transcriptional multivariate dependency of genes, hereafter referred to as the global coordination level (GCL), without inferring the whole network of pairwise correlations. The GCL analysis measures the average multivariate dependency between expression levels of random gene subsets of single cells. To calculate the GCL, we first divide the genes into two random subsets. Then we measure the dependency level between the two subsets over a cohort of cells. In this study, we use

the ‘bias-corrected distance correlation’ (bcdCorr)<sup>30</sup> (Methods), but essentially any high-dimensional dependency measure can be used. The meaning of high bcdCorr is that similarity between the expression profiles of two random cells in one subset of genes is associated with their similarity in the other subset of genes, whereas a difference in one subset is associated with a difference in the other subset. Such association may indicate an overall level of coordination between the genes in the two subsets. Finally, we repeat these steps for different random subsets and define the GCL as the average of the dependency levels.

For a large sample size, the empirical GCL is bounded between zero and one: zero corresponds to the case of independent gene expression, whereas a significantly non-zero GCL reflects coordinated transcriptional expression, which could be interpreted as a result of underlying molecular dynamics, such as gene-to-gene regulatory interactions.

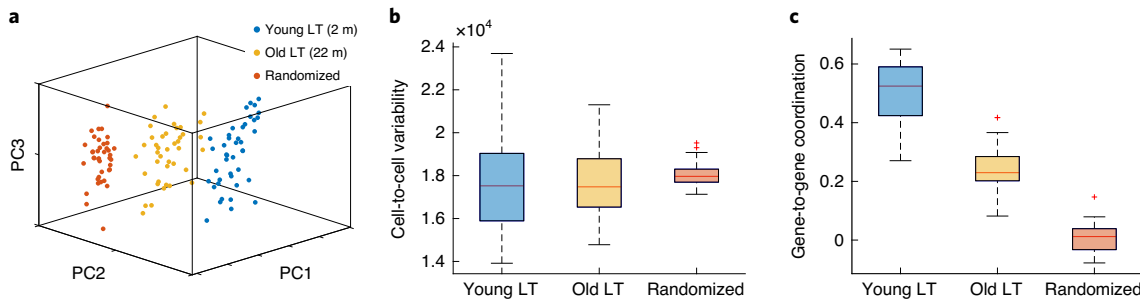


**Fig. 1 | Loss of gene-to-gene coordination in ageing LT-HSCs.** **a**, PCA visualization of LT-HSCs' transcriptomes from young (2–3 months) and old (22–24 months) mice<sup>34</sup> together with randomized transcriptomes with respect to the old ones (as described in Extended Data Fig. 2). Blue and yellow points represent the transcriptomes of young and old single cells, respectively. Red points represent randomized transcriptomes and are horizontally shifted for visualization purposes. In randomized transcriptomes any effect of gene-to-gene interactions, if present in real cells, is effectively removed. **b**, Cell-to-cell variability, measured as Euclidean distance between each transcriptome and the average transcriptome<sup>16</sup>, of the three groups (young, old and randomized) is roughly the same. **c**, Gene-to-gene coordination level, measured as GCL, is significantly lower in the old cells compared with the young cells and close to zero for randomized data. Box plots represent the distributions of GCL values calculated for 30 bootstrap realizations, each consists of 20 transcripts. Centre line, median; box limits, upper and lower quartiles; whiskers, 1.5× interquartile range; points, outliers.

As an illustration of the coordination measured by the GCL, consider the expression profiles of cells with  $N$  genes that are represented as points in an  $N$ -dimensional space. If the gene expression levels are not independent, the set of points do not fill the  $N$ -dimensional space but are rather located near a lower-dimensional manifold (Extended Data Fig. 1). The low-dimensional manifold represents a general form of transcriptional dependency, including non-linear and high-order relations. In a sense, in analogy with Pearson correlation, where the correlation strength is represented by the closeness of the data points to a straight line, the GCL measures the dependency level of genes, which is represented by the closeness of the points (cells) to a low-dimensional dependency manifold. However, while the Pearson coefficient measures a specific, linear correlation form, in the GCL the form of the manifold is assumed to be unknown and is not calculated. The GCL measure has two main advantages. (1) The dependency level is defined with respect to a general dependency form, not specific relations (such as linear); thus, it can measure relations between variables even where the correlation is zero, as demonstrated in Extended Data Fig. 1. (2) It can include high-order dependencies between multiple variables.

To demonstrate that the GCL is a measure of the transcriptional dependency between genes, we first applied it to data from a cohort of long-term HSCs<sup>31</sup> (LT-HSCs) before and after shuffling the expression levels of each gene independently across the cells (Extended Data Fig. 2a–c and Supplementary Information). The shuffling procedure effectively removes any effect of gene-to-gene dependency but preserves the other statistical features of the data; that is, the expression distribution of each gene. Indeed, the GCL value of the real data was significantly higher than that of the shuffled data, which is practically zero (a two-sided Student's *t*-test between the distributions of 200 bootstrap realizations yields  $P < 10^{-100}$ ).

Next, we asked whether transcriptional coordination is associated with functional relations between genes. We systematically analysed 170 pathways (according to the Kyoto Encyclopedia of Genes and Genomes<sup>32</sup> (KEGG)) in LT-HSCs from three independent studies<sup>31,33,34</sup>. We compared the GCL value of each pathway to the GCL values of corresponding 'surrogate' gene sets. These surrogate gene sets were randomly selected from a subset of genes with similar expression levels as the pathway's genes. Thus, each surrogate gene set preserves the size of the original pathway and mimics its expression profile, but does not represent any known KEGG pathway (see Methods and Extended Data Fig. 4d–f for a detailed explanation of the surrogate procedure). By analysing the distribution of GCL values of the pathway compared with the distribution

of the surrogate gene sets, we aimed to test whether the former tend to have elevated coordination.

As the GCL values of the surrogate gene sets associated with the same pathway roughly follow a normal distribution, we calculated a Z score for each pathway with respect to surrogate gene sets. For example, in the null expectation that is, if there was no additional coordination between genes of the same pathway, only approximately 16% of the pathways in each dataset would be expected to have a Z score of  $>1$ , similarly to the surrogate gene sets. As shown in Extended Data Fig. 4g–i, the portion of pathways with a  $Z > 1$  is significantly larger in each of the three studies (28% in Kowalczyk et al.<sup>33</sup>, 26% in Mann et al.<sup>31</sup> and 25% in Grover et al.<sup>34</sup>). The GCL value and the associated Z score calculated for each particular pathway do not conclusively indicate the coordination level between the genes of that pathway because of the limited statistical power of the GCL when calculated over a relatively small number of genes. Nevertheless, the total large number of pathways with elevated Z scores indicates an association between elevated gene-to-gene coordination and functional relation between genes. Moreover, the proportion of the overlapping pathways—that is, pathways with  $Z > 1$  in all three different studies—is roughly 8%, significantly higher than the roughly 1.8% expected in the case of independent studies (Extended Data Fig. 4j,k), suggesting that the lists of pathways with higher GCL values in the different studies are not independent.

**Loss of gene-to-gene transcriptional coordination during ageing.** Next, we systematically analysed the changes of gene-to-gene transcriptional coordination in 20 cohorts of scRNA-seq data from seven different studies of ageing single cells. These cohorts represent very different species (fruit fly, mouse and human) and very different cell types (HSCs, immune cells, pancreatic cells, neurons and glial cells) (see Table 1 for a detailed description). For each cohort, we compared the GCL values of cells from young and old organisms. To minimize the effects of potential confounding factors related to different experimental setups, bioinformatics pipelines or cell-type-specific regulatory dynamics, we directly compared only GCL values calculated for cells of the same type and organism and from the same study. Figure 1 shows the transcriptional changes in ageing mice LT-HSCs as reported in ref.<sup>34</sup>, as well as in randomized data (with respect to the old transcriptomes). While the cell-to-cell variability (squared Euclidean distances between each cell and the average cell, following ref.<sup>16</sup>; see Methods) was practically the same in all three groups (young, old and randomized), the gene-to-gene coordination significantly decreased with age. These results

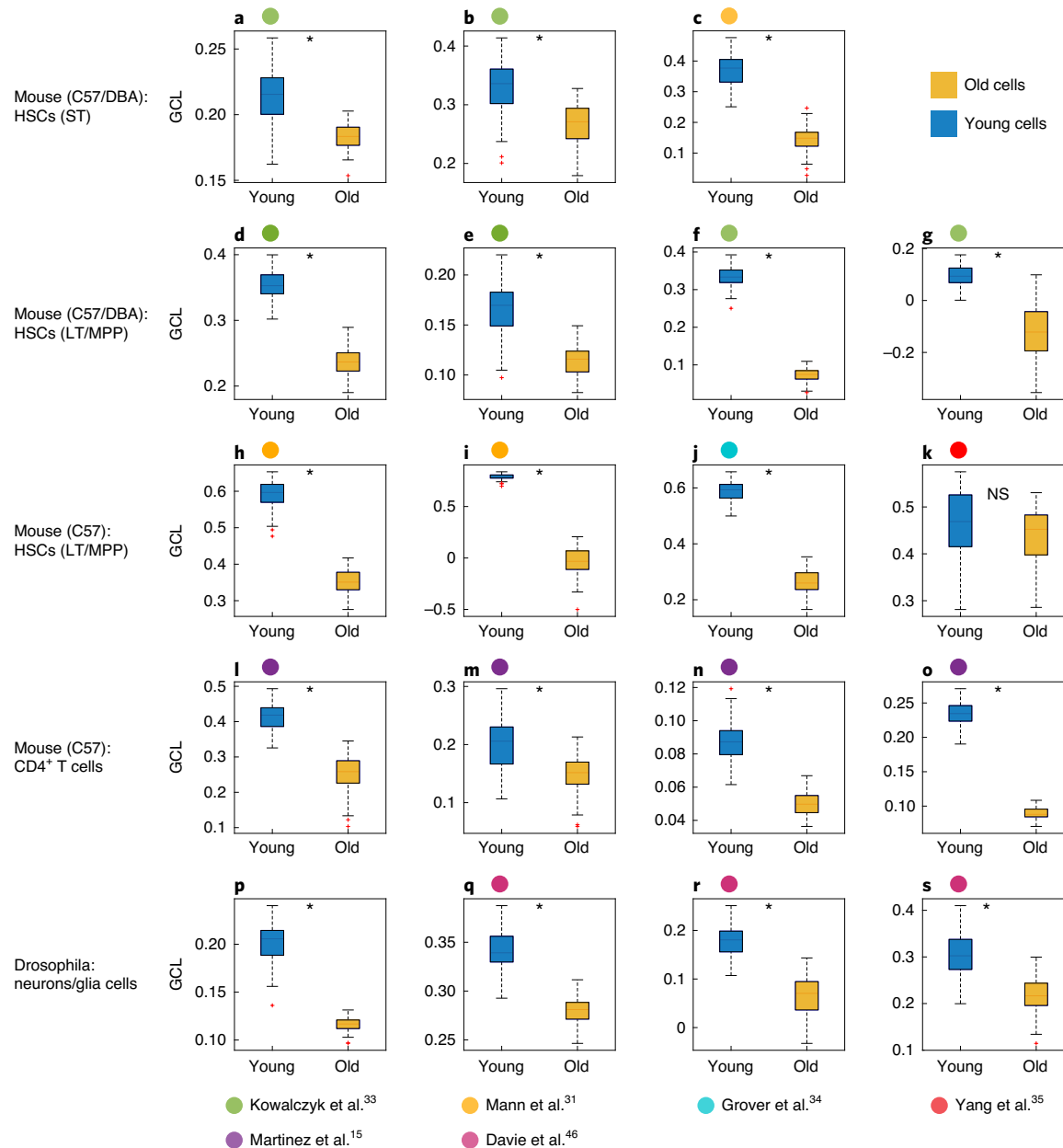


**Fig. 2 | Ageing associated reduction of GCL in different tissues and cell types across various studies.** Comparison of GCL values of cells from young and old organisms (blue and yellow boxes, respectively). The boxes show the GCL values calculated for  $M=100$  bootstrap realizations for each group of cells (here we set  $M=100$ ; see Methods and Extended Data Fig. 2). **a–c**, ST-HSCs from C57 mice (**a**) and DBA mice (**b**), both from ref. <sup>33</sup>; and from C57 (**c**) from ref. <sup>31</sup>. **d–s**, LT-HSCs from C57 mice (**d**) and DBA mice (**e**); MPP-HSCs from C57 mice (**f**) and DBA mice (**g**) from ref. <sup>33</sup>; LT-HSCs (**h**) and MPP-HSCs (**i**) from C57 mice from ref. <sup>31</sup>; LT-HSCs from C57 mice from ref. <sup>34</sup> (**j**) and MPP-HSCs from C57 mice from ref. <sup>46</sup> (**k**); mouse immune CD4<sup>+</sup> T cells, stimulated effector memory cells (**l**); stimulated naïve cells (**m**); unstimulated naïve cells (**n**) and unstimulated effector memory cells (**o**) from ref. <sup>15</sup>; *Drosophila melanogaster* glia cells—‘astrocyte-like’ (**p**), ‘ensheathing’ (**q**) and *Drosophila* neurons—neurons of the optic lobes (Dm8.Tm5c) (**r**) and antero-dorsal olfactory projection neurons (OPN.adPNandPN) (**s**) from ref. <sup>45</sup>. The clear tendency of reduction of GCL values in old cells compared with young cells (in most cases) indicates a general loss of gene-to-gene coordination with age. Centre line, median; box limits, upper and lower quartiles; whiskers, 1.5x interquartile range; points, outliers. \* $P < 10^{-10}$  using two-tailed, unpaired, unequal variance t-test; NS,  $P > 10^{-3}$ , adjusted for multiple comparisons by the Bonferroni procedure. The number of cells in each group is reported in Table 1. Exact P values are reported in Table 2.

demonstrate that the two suggested measures for age-related transcriptional dysregulation, gene-to-gene coordination and cell-to-cell variability, are effectively independent measures, with ageing HSCs being characterized by decreased gene-to-gene coordination but an undetectable increase in cell-to-cell variability. Additionally, we demonstrate the independence of these measures by manipulating synthetic data. We show that the addition of noise to a cohort of

cells could be practically masked by the natural cell-to-cell variability but noticeably affect the gene-to-gene coordination (Extended Data Fig. 4).

The GCL analyses of 19 cohorts of scRNA-seq data from mice and fruit flies, from six different studies, are shown in Fig. 2 (human pancreas cells are analysed in a separate section). Specifically, we analysed five types of mouse cell, (1) short-term- (ST)-HSCs, (2)

**Table 2 | Summary of all datasets and all types of analysis ageing associated reduction of GCL in different tissues and cell types across various studies calculated using top 2,000–4,000 expressed genes**

Cell type	No. of cells		No. of genes with DEGs			No. of genes without DEGs		
	Old	Young	2,000	3,000	4,000	2,000	3,000	4,000
STHC, C57BL6, Kowalczyk et al. <sup>33</sup>	227	118	<b>2.10 × 10<sup>-40</sup></b>	<b>3.14 × 10<sup>-30</sup></b>	<b>1.80 × 10<sup>-36</sup></b>	<b>1.95 × 10<sup>-46</sup></b>	<b>3.31 × 10<sup>-24</sup></b>	<b>9.48 × 10<sup>-27</sup></b>
LTHSC, C57BL6, Kowalczyk et al. <sup>33</sup>	199	113	<b>1.71 × 10<sup>-12</sup></b>	<b>7.92 × 10<sup>-96</sup></b>	<b>3.42 × 10<sup>-90</sup></b>	<b>3.39 × 10<sup>-82</sup></b>	<b>1.06 × 10<sup>-75</sup></b>	<b>2.36 × 10<sup>-90</sup></b>
Ensheathing glia, Davie et al. <sup>45</sup>	166	112	<b>4.14 × 10<sup>-58</sup></b>	<b>1.20 × 10<sup>-61</sup></b>	<b>3.94 × 10<sup>-71</sup></b>	<b>2.55 × 10<sup>-82</sup></b>	<b>3.00 × 10<sup>-54</sup></b>	<b>2.69 × 10<sup>-79</sup></b>
FpEUnstim, Martinez et al. <sup>15</sup>	115	109	<b>1.31 × 10<sup>-120</sup></b>	<b>1.45 × 10<sup>-124</sup></b>	<b>2.35 × 10<sup>-116</sup></b>	<b>3.68 × 10<sup>-125</sup></b>	<b>5.49 × 10<sup>-107</sup></b>	<b>9.53 × 10<sup>-131</sup></b>
FpUnstim, Martinez et al. <sup>15</sup>	121	90	<b>3.46 × 10<sup>-68</sup></b>	<b>8.19 × 10<sup>-67</sup></b>	<b>9.04 × 10<sup>-72</sup></b>	<b>4.41 × 10<sup>-50</sup></b>	<b>2.63 × 10<sup>-54</sup></b>	<b>6.22 × 10<sup>-77</sup></b>
Astrocyte-like, Davie et al. <sup>45</sup>	269	66	<b>4.13 × 10<sup>-58</sup></b>	<b>5.98 × 10<sup>-71</sup></b>	<b>3.13 × 10<sup>-49</sup></b>	<b>1.22 × 10<sup>-68</sup></b>	<b>7.01 × 10<sup>-47</sup></b>	<b>2.49 × 10<sup>-58</sup></b>
MPP, C57BL6, Kowalczyk et al. <sup>33</sup>	46	76	<b>2.64 × 10<sup>-131</sup></b>	<b>1.50 × 10<sup>-144</sup></b>	<b>5.67 × 10<sup>-145</sup></b>	<b>2.66 × 10<sup>-143</sup></b>	<b>1.43 × 10<sup>-138</sup></b>	<b>1.68 × 10<sup>-171</sup></b>
STHSC, DBA/2, Kowalczyk et al. <sup>33</sup>	45	46	<b>5.29 × 10<sup>-27</sup></b>	<b>1.32 × 10<sup>-23</sup></b>	<b>3.57 × 10<sup>-32</sup></b>	<b>6.68 × 10<sup>-41</sup></b>	<b>1.85 × 10<sup>-31</sup></b>	<b>5.59 × 10<sup>-34</sup></b>
LTHSC, DBA/2, Kowalczyk et al. <sup>33</sup>	54	44	0.735	<b>2.19 × 10<sup>-37</sup></b>	<b>7.10 × 10<sup>-28</sup></b>	<b>1.54 × 10<sup>-17</sup></b>	<b>8.37 × 10<sup>-11</sup></b>	<b>5.44 × 10<sup>-40</sup></b>
LT, Mann et al. <sup>31</sup>	42	51	* <b>2.31 × 10<sup>-47</sup></b>	<b>1.98 × 10<sup>-109</sup></b>	<b>2.30 × 10<sup>-114</sup></b>	<b>3.88 × 10<sup>-113</sup></b>	<b>9.28 × 10<sup>-90</sup></b>	<b>1.25 × 10<sup>-112</sup></b>
Dm8.Tm5c, Davie et al. <sup>45</sup>	32	39	<b>2.70 × 10<sup>-30</sup></b>	<b>1.27 × 10<sup>-57</sup></b>	<b>3.69 × 10<sup>-57</sup></b>	<b>6.65 × 10<sup>-38</sup></b>	<b>2.03 × 10<sup>-52</sup></b>	<b>7.11 × 10<sup>-13</sup></b>
LT, Grover et al. <sup>34</sup>	31	47	<b>1.66 × 10<sup>-101</sup></b>	<b>7.76 × 10<sup>-129</sup></b>	<b>2.58 × 10<sup>-118</sup></b>	<b>2.93 × 10<sup>-105</sup></b>	<b>3.57 × 10<sup>-122</sup></b>	<b>2.64 × 10<sup>-125</sup></b>
FpActive, Martinez et al. <sup>15</sup>	36	30	0.862	<b>3.20 × 10<sup>-18</sup></b>	<b>9.18 × 10<sup>-36</sup></b>	<b>3.14 × 10<sup>-35</sup></b>	<b>6.70 × 10<sup>-23</sup></b>	<b>5.83 × 10<sup>-24</sup></b>
ST, Mann et al. <sup>31</sup>	38	29	* <b>1.50 × 10<sup>-98</sup></b>	<b>2.31 × 10<sup>-85</sup></b>	<b>4.12 × 10<sup>-70</sup></b>	<b>3.85 × 10<sup>-50</sup></b>	<b>2.25 × 10<sup>-74</sup></b>	<b>1.80 × 10<sup>-65</sup></b>
FpEActive, Domesticus, Martinez et al. <sup>15</sup>	29	26	<b>1.10 × 10<sup>-81</sup></b>	<b>5.94 × 10<sup>-66</sup></b>	<b>9.54 × 10<sup>-77</sup></b>	<b>1.36 × 10<sup>-69</sup></b>	<b>1.50 × 10<sup>-70</sup></b>	<b>5.20 × 10<sup>-76</sup></b>
OPN.adPNandIPN, Davie et al. <sup>45</sup>	22	24	* <b>1.77 × 10<sup>-105</sup></b>	<b>3.81 × 10<sup>-32</sup></b>	<b>7.31 × 10<sup>-60</sup></b>	<b>3.03 × 10<sup>-26</sup></b>	<b>3.55 × 10<sup>-11</sup></b>	<b>8.67 × 10<sup>-34</sup></b>
MPP, Mann et al. <sup>31</sup>	21	56	0.196	<b>2.19 × 10<sup>-86</sup></b>	<b>4.08 × 10<sup>-77</sup></b>	<b>6.10 × 10<sup>-85</sup></b>	<b>2.37 × 10<sup>-92</sup></b>	<b>9.32 × 10<sup>-80</sup></b>
MPP, Young et al. <sup>46</sup>	20	23	0.3688	0.003	<b>1.06 × 10<sup>-5</sup></b>	<b>1.09 × 10<sup>-46</sup></b>	<b>5.74 × 10<sup>-19</sup></b>	<b>0.002</b>
MPP, DBA/2, Kowalczyk et al. <sup>33</sup>	16	27	<b>2.63 × 10<sup>-64</sup></b>	<b>1.89 × 10<sup>-41</sup></b>	<b>1.81 × 10<sup>-17</sup></b>	<b>5.80 × 10<sup>-16</sup></b>	<b>2.16 × 10<sup>-49</sup></b>	<b>1.85 × 10<sup>-26</sup></b>

The table numbers are the precise P values based on two-tailed, unpaired, unequal variance Student's t-test. Bold text represents a significant reduction of GCL, italic text (\*) represents a significant increase of GCL and roman text represents an insignificant change ( $P > 0.05$ ). As explained in the Supplementary Information, ageing and the results of decreased GCL during ageing are consistent across the different conditions and parameters.

LT-HSCs, (3) multipotent progenitor (MPP) HSCs, (4) unstimulated/stimulated naïve CD4<sup>+</sup> T cells and (5) unstimulated/stimulated effector memory CD4<sup>+</sup> T cells, two types of *Drosophila* glial cell, (6) ‘ensheathing’ and (7) ‘astrocyte-like’, and two types of *Drosophila* neuron, (8) antero-dorsal olfactory projection neurons (OPN.adPNandIPN) and (9) neurons of the optic lobes (Dm8.Tm5c) (see Methods for details of the datasets, including organisms’ ages). For each cohort, we calculated the GCL over the top 3,000 expressed genes for cells from young and old organisms. We find a significant age-related decrease in the GCL across cell types and organisms. As discussed in the Supplementary Information and shown in Supplementary Figs. 2 and 3, our results remain consistent also when analysing top 2,000 or top 4,000 expressed genes.

To verify the pattern of reduced coordination is not a direct result of genes age-related deterministic changes that tend to repeat across different individual cells, we removed the differentially expressed genes (DEGs) between the young and old cohorts. The DEGs represent an ‘ageing signature’, a characteristic transcriptional pattern that discriminates the old from the young cells. By contrast, the ‘non-DEGs’ manifest processes that affect each individual cell differently. As discussed in Supplementary Information and shown in Supplementary Figs. 3–5 and Table 2, we find consistent results, that is, age-related reduction of GCL in the non-DEGs across the different cell types. We also calculated the age-related changes in cell-to-cell transcriptional variability, defined for each gene separately as in ref. <sup>15</sup> (Methods and Extended Data Fig. 5) and for the whole genome as in ref. <sup>16</sup>, for each of the cohorts (Extended Data Fig. 6). While the cell-to-cell variability increases in ageing cells in several cases, this observation does not represent a general attribute of ageing, as shown before<sup>22</sup>.

We note that, in a general case, an observed difference between two GCL values from a particular pair of cohorts does not necessarily suggest that their coordination levels are different. Alternatively, different GCL values could be interpreted as a result of other factors, such as differences in a characteristic of their underlying dynamics. In our case, however, the fact that (1) the same direction of change, that is, reduction of the GCL, is observed across 19 different pairs of cohorts, together with (2) the previous observations of increased disorder in ageing cells, that is, accumulated stochastic genetic errors and increased transcriptional variability in part of the cell types, strongly indicate interpreting the consistent reduction of GCL as an ageing-related loss of gene-to-gene coordination.

In summary, our results show a consistent pattern of reduced GCL values in cells from old organisms compared with cells from young organisms, indicating universal processes of transcriptional dysregulation in ageing.

**Loss of gene-to-gene coordination is associated with ageing-related DNA damage.** The accumulation of cellular damage is considered to be a general cause of ageing<sup>8</sup>. A fundamental question is whether transcriptional dysregulation during ageing is directly linked to damage accumulation, or alternatively, these are two independent characteristics of ageing. Specifically, it has been previously suggested that somatic mutations, especially large genome rearrangements, can have a direct causative role in transcriptional dysregulation<sup>7</sup>. However, this relation has not yet been demonstrated in single-cell data. Moreover, recent experimental findings seem to suggest that ageing is characterized by both accumulations of genetic mutations and transcriptional dysregulation (in terms of cell-to-cell variability) in an independent fashion<sup>16</sup>. Here, we asked

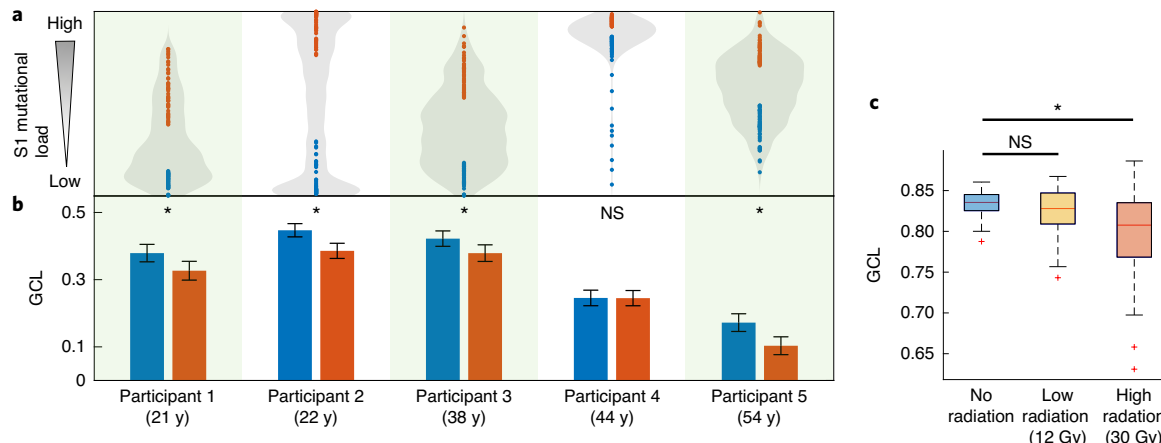


**Fig. 3 | Increased mutational load of signature S1 and high irradiation are associated with decreased gene-to-gene coordination.** **a**, Human pancreas glucagon cells from five participants are ranked according to their load of S1 signature (high rate of C > A, followed by C > G and C > T substitutions), as defined in ref. <sup>16</sup>. Rank distributions of each participant are shown in grey and the top- and bottom-ranked 50 cells of each participant are marked in red and blue circles, respectively. For participants 1 ( $n=157$ ), 2 ( $n=133$ ), 3 ( $n=226$ ) and 5 ( $n=171$ ) the rank of S1 mutational load is heterogeneous among cells from the same participant, with substantial differences between the top- and bottom-ranked cells. In contrast, the rank of S1 mutational load in the cells of participant 4 ( $n=141$ ) is considerably homogenous. **b**, Gene-to-gene coordination (GCL value) was calculated for the top- and bottom-ranked cells of each participant separately. Bar heights, GCL values (calculated using bcdcorr on  $n=50$  random genes division); error bars, standard deviation of the corresponding ‘bias-corrected distance correlation’ values ( $m=50$ ); \* $P<10^{-10}$  using a two-tailed, unpaired, unequal variance t-test; NS,  $P>10^{-3}$ . For participants 1, 2, 3 and 5, there is a clear reduction of GCL values with increasing of S1 mutational load. For participant 4, the S1 mutational load of the cells is similar and, accordingly, the GCL values of the top and bottom cells are similar. **c**, GCL values of ‘no-radiation’ ( $n=41$  biological independent samples), ‘low-radiation’ (12 Gy) ( $n=88$  biological independent samples) and ‘high radiation’ (30 Gy) ( $n=89$  biological independent samples) groups of cells from ref. <sup>35</sup>. The boxes show the GCL values calculated for 100 bootstrap realizations for each group of cells. Box limits, upper and lower quartiles; whiskers, 1.5x interquartile range; points, outliers; centre line, median. \* $P<10^{-5}$  using two-tailed, unpaired, unequal variance t-test; NS,  $P>0.05$ .

whether decreased gene-to-gene transcriptional coordination is linked to the accumulation of genetic damage.

To address this, we analysed two datasets of scRNA-seq and compared, in each dataset, the GCL calculated for cohorts of cells with different levels of genetic damage. In one dataset, cells accumulated genetic substitutions while in the other dataset, cells were exposed to high levels of radiation.

First, we analysed the relation between mutational load and gene-to-gene coordination within cohorts of cells taken from the same human participant, that is, they are all associated with the same chronological age of the organism. If gene-to-gene coordination is linked to genetic mutations, we expect a lower GCL value for cells with higher mutational load. If, however, the two age-related processes, that is, reduced gene-to-gene coordination and accumulation of genetic mutations, are practically independent, a significant change in the GCL values as a function of mutational load is not expected among cells from the same human participant.

We analysed scRNA-seq data of human endocrine pancreas cells from five participants aged 21, 22, 38, 44 and 54 years<sup>16</sup>. The cells of all the participants were ordered according to the fraction of mutations attributed to signature S1, a pancreas-specific mutational signature that is characterized by C > A, C > G and C > T substitutions found to accumulate in ageing cells<sup>16</sup> (the other mutational signatures S2 and S3 appeared in an insufficient number of cells to be analysed by GCL). Here, for each individual participant, we calculated the GCL values for the 50 cells with the highest S1 rank and for the 50 cells with the lowest S1 rank (Fig. 3a). As shown in Fig. 3b, in four out of the five participants, the GCL values of the cells with a lower S1 load were significantly higher than those of cells with high S1 load ( $P<10^{-14}$  using a two-tailed, unpaired, unequal variance t-test). The only exception was participant 4 (44 years old), for whom the S1 signature rankings of the cells were narrowly distributed, compared with the other participants, and the GCL values of the top and bottom ranking cells were almost equal

( $P>0.4$ ). Taken together, the results from all five participants show an ageing-independent link between mutational load of S1 signature and reduction of gene-to-gene coordination.

This observed association between genetic substitutions and loss of transcriptional gene-to-gene coordination does not necessarily mean a direct causative relation but could be due to other factors. For example, epigenetic errors may be the cause of transcriptional dysregulation while they have been accumulating in the same individual cells with a high number of genetic substitutions. Further data on both genetic and epigenetic errors in single cells are required to address this question.

Second, we analysed recent scRNA-seq data from an experimental study of cells exposed to radiation<sup>35</sup>. Gene-expression profiles of oesophageal squamous cell carcinoma single cells with and without fractionated irradiation have been measured after 3 d of recovery. Specifically, a total of 218 scRNA-seq expression profiles were obtained from three groups of cells exposed to 12 or 30 Gy, and cells not exposed to radiation. In addition, the study shows that the expression of γ-H2AX, a marker of irradiation-induced double-strand breaks, dramatically increased 2 h after the oesophageal squamous cell carcinoma cells were exposed to additional 4 Gy of radiation; thus, the cells irradiated by 12 or 30 Gy are considered to have corresponding levels of genetic damage.

We measured the GCL in the three groups of cells: ‘no-radiation’, ‘low-radiation’ (12 Gy) and ‘high radiation’ (30 Gy). As shown in Fig. 3c, the GCL values calculated for the ‘high radiation’ group are significantly lower compared with ‘no-radiation’ and ‘low-radiation’ groups. This result indicates a connection between radiation-induced DNA damage and reduced GCL, while the perturbation experiment may indicate a causal link between them.

Here we offer a possible mechanistic interpretation of such a link. In each individual cell, the accumulation of random genetic aberrations can damage regulatory elements, such as promoter and enhancer elements as well as exonic sequences. Since the

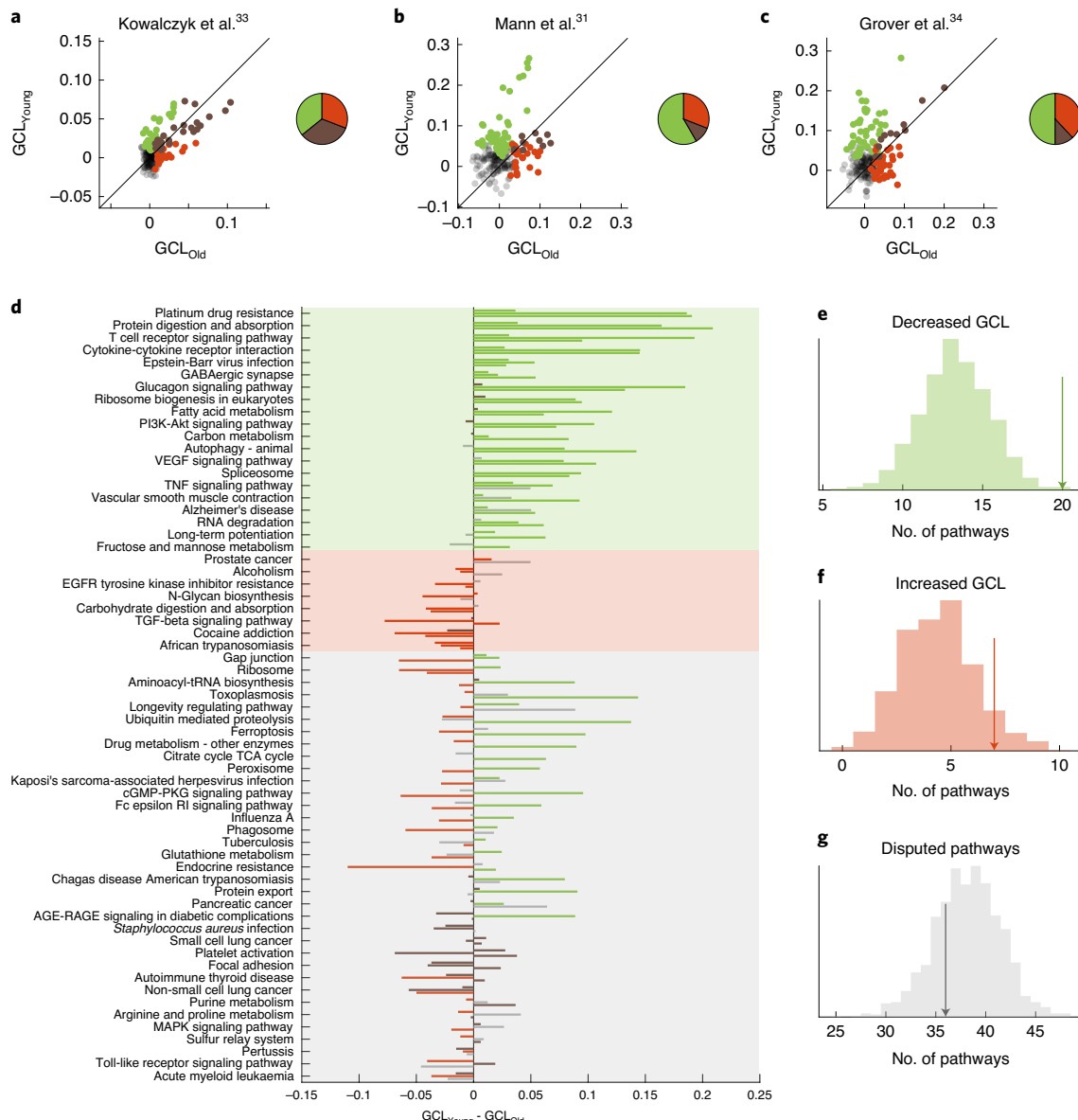


**Fig. 4 | Cross-datasets pathway analysis reveals the characteristic ageing effect in LT-HSCs.** **a–c**, Young versus old GCL values of pathways show a tendency of decreased GCL of pathways during ageing. Green, red and brown circles represent a pathway with decreased, increased and unchanged GCL values during ageing, respectively (the ratios of the three categories are represented by the pie charts). Grey circles represent pathways with no significant GCL ( $Z < 1$ ) in both young and old. **d**, Validation of GCL changes across datasets: 63 pathways were found to have a notable GCL value in at least two studies. Three bars for each pathway represent the GCL differences in ref. <sup>33</sup> (top), ref. <sup>31</sup> (middle) and ref. <sup>34</sup> (bottom), whereas the colours of the bars are the same as the corresponding circles in **a–c**. Pathways with validated ‘decreased GCL’, ‘increased GCL’ and ‘unchanged’ are marked with green, red and grey backgrounds, respectively. **e–g**, We report one-tailed  $P$  values for each category, calculated as the fraction of null-model realizations (histograms, see Methods) with a number of pathways equal to or larger than the number in the original data (arrows). The pathways that exhibit a ‘decreased GCL’ effect tend to preserve this feature across datasets (**e**),  $P < 10^{-3}$ , in contrast with the pathways of the other categories (**f,g**), suggesting that the pathways in this category are more susceptible to reduced gene-to-gene coordination during ageing.

regulatory system of each cell is affected differently, the group-effect in a cohort of cells, or a tissue, will be an effective reduction in the transcriptional gene-to-gene coordination. A causal link between genetic damage and transcriptional dysregulation was previously demonstrated, where treating cells isolated from young animals with hydrogen peroxide produced an increase in expression variability of individual genes<sup>13</sup>. Our result of reduced GCL in whole-genome transcription data of cells exposed to high radiation supports this conclusion.

To illustrate how random aberrations of gene regulatory elements can affect the GCL measure, we applied it to synthetic data

generated by eight qualitatively different mathematical models of gene regulation<sup>23,36–38</sup> (Methods). We generated ‘cohorts’ of ‘expression profiles’ with a controlled amount of random variations in the generated model, specifically, in the terms representing the interactions between the genes. Extended Data Fig. 7 shows that a larger number of random variations in the underlying regulatory networks is accompanied by a decrease in the GCL value.

In addition, as shown in Fig. 3a,b, the GCL values of the older participants (ages 44 and 54) are lower than those of the younger participants (ages 21–38). This comparison between human participants of different ages should be interpreted with caution because,

unlike the cohorts of cells from animal models shown above (Fig. 2), different human participants generally do not share similar genetic backgrounds and environmental conditions, a fact that can introduce considerable noise. Nevertheless, these results of a gradual loss of gene-to-gene coordination in ageing humans are in agreement with the results of the animal models.

**Age-related changes of gene-to-gene coordination across pathways.** Finally, we asked whether the general effect of transcriptional coordination reduction, observed over the entire transcriptome, appears equally across different pathways or whether there are some pathways that are more susceptible than others. Specifically, we investigated this by calculating the age-related changes of GCL values of 170 KEGG pathways across three different studies of LT-HSCs in mouse, independently<sup>31,33,34</sup>. In each study, the age-related changes vary across the different pathways, where more pathways exhibit an age-related reduction of GCL than an age-related increase of GCL (Fig. 4a–c). Such variance could be random due to the relatively small number of genes in each pathway, but may also reflect a characteristic tendency associated with specific cellular functions.

To address this question, we compared the changes of GCL of each pathway across the three different studies. A significant agreement between the results from the different studies would indicate that the variance of GCL changes across pathways is not random. First, in each study, we classified each pathway into one of four categories: ‘decreased GCL’, ‘increased GCL’, ‘unchanged’ and ‘insignificant’ (green, red, brown and grey circles in Fig. 4a–c; see Methods). Then, we compared the four categories of pathways concluded from the three studies. Figure 4d compares the GCL differences shown in Fig. 4a–c, where the colour of each bar represents the pathway category in each study. We found a high agreement of the pathway categorized as ‘decreased GCL’ across different studies (Fig. 4e). This is evident from the significantly large number of pathways for which the studies agree (20 pathways), compared with the expected number in case of no consistency of the analysis across studies (approximately 13 pathways). A considerably large number of pathways that exhibit transcriptional dysregulation using the GCL method are also known to be associated with ageing in different aspects, for example, the PI3K-Akt signalling pathway<sup>39</sup>. By contrast, for the other categories (Fig. 4f,g), we found no evidence for significant agreement across studies, meaning that the pathways for which the GCL was higher in old than young mice probably represent random fluctuations rather than a stable biological signal.

These findings indicate that, despite the stochastic nature of the transcriptional dysregulation, the loss of transcriptional coordination in terms of reduced GCL is not random, but some specific cellular functions are more susceptible than others. Future research is required to determine whether this susceptibility is due to structural features of the pathways, for example, a large number of gene regulatory elements that become a larger target for mutations and epi-mutations, or due to higher rate of damage accumulation, for example, less effective activity of protective and maintenance mechanisms.

## Discussion

While the concept of transcriptional dysregulation has been proposed to be a possible central mechanism of functional decline during ageing, until now its generality has not been comprehensively empirically supported. It has been previously found in terms of reduced coexpression in bulk data from a set of tissues<sup>34</sup> and in terms of increased transcriptional variability in single cells<sup>3,15–17</sup>. However, these findings either disregard the stochastic differences between the individual cells, or were limited for specific cell types and specific tissues. By focusing on the dependencies between the genes in a ‘top-down’ approach, we observed an age-related decline

of transcriptional gene-to-gene coordination across different organisms and very different cell types, including mitotically active and postmitotic cells. These observations confirm that transcriptional dysregulation is a general and fundamental attribute of ageing.

This general finding could have important implications for the efforts to develop therapies for ageing. Transcriptional dysregulation in the form of reduced gene-to-gene coordination may reflect a stochastic process that broadly disrupts many cells in the tissue, as opposed to a small portion of ‘ageing cells’ with specific disrupted elements, for example shortening telomeres or programmed responses, such as apoptosis or senescence. Therefore, if transcriptional dysregulation is indeed a prime mechanism that links the stochastic somatic damage and the decline of tissue function, healthy ageing therapies could not focus only on fixing the known specific mechanisms, but face the more substantial challenge of preventing or slowing down the accumulation of somatic damage.

Finally, we anticipate that applying our GCL measure to other scRNA-seq studies will offer deeper insights into gene-to-gene coordination even where the gene regulatory network (GRN) is not known. Specifically, the GCL can be applied to study biological processes that involve random damage, such as progeroid syndromes or cancer.

## Methods

**Bias-corrected distance correlation (bcdCorr).** The dependency level between two variables can be evaluated via the bcdCorr<sup>40</sup>, a refined version of the distance correlation<sup>40</sup> (dCorr). In brief, the distance correlation evaluates the level of dependence between two variables by testing how the distance between two samples as measured by one variable is changed compared to the distance between the two samples as measured by the other variable. In other words, a high level of dependency means that small changes in one variable are associated with small changes in the other variable. This measure can capture non-linear relationships that are not detectable with conventional correlation methods. For example, the correlation between two quadratically related variables, for example,  $y = x^2$  where  $x$  is symmetrically distributed around zero, is zero. However, when comparing two samples, that is, to data points  $(x_i, y_i)$  and  $(x_j, y_j)$ , it is obvious that the difference between the two samples in one dimension ( $|x_i - x_j|$ ) is correlated with the difference in the second dimension ( $|y_i - y_j|$ ). Similarly, the distance correlation can also be applied to measure the dependency between two high-dimensional variables.

Consider  $M$  observations of two high-dimensional variables  $X_i \in \mathbb{R}^p$  and  $Y_i \in \mathbb{R}^q$ ,  $i = 1, \dots, M$ , where  $X_i = (X_{i,1}, \dots, X_{i,p})$  and  $Y_i = (Y_{i,1}, \dots, Y_{i,q})$ . Note that  $q$  does not necessarily have to be equal to  $p$ . The  $M$  observations are represented by the  $p \times M$  matrix  $X$  and  $q \times M$  matrix  $Y$ . The empirical bcdCorr( $X, Y$ ) is defined as

$$\text{bcdCorr}(X, Y) = \frac{\text{dCov}(X, Y)}{\sqrt{\text{dCov}(X, X) \times \text{dCov}(Y, Y)}} \quad (1)$$

where

$$\text{dCov}(X, Y) = \frac{1}{M(M-3)} \left[ \sum_{i,j=1}^M A_{i,j}^* B_{i,j}^* - \frac{M}{M-2} \sum_{i=1}^M A_{i,i}^* B_{i,i}^* \right] \quad (2)$$

and  $A_{i,j}^*$  and  $B_{i,j}^*$  are matrices defined as

$$A_{ij}^* = \begin{cases} \frac{M}{M-1} (A_{i,j} - \bar{a}_{ij}), & i \neq j \\ \frac{M}{M-1} (\bar{a}_i - \bar{a}), & i = j \end{cases}, \quad B_{ij}^* = \begin{cases} \frac{M}{M-1} (B_{i,j} - \bar{b}_{ij}), & i \neq j \\ \frac{M}{M-1} (\bar{b}_i - \bar{b}), & i = j \end{cases} \quad (3)$$

and  $A_{i,j}$  and  $B_{i,j}$  are matrices defined as

$$A_{i,j} = a_{ij} - \bar{a}_i - \bar{a}_j + \bar{a}, \quad (4)$$

$$B_{i,j} = b_{ij} - \bar{b}_i - \bar{b}_j + \bar{b} \quad (5)$$

where

$$a_{ij} = |X_i - X_j|, \quad i, j = 1, \dots, M, \quad (6)$$

$$a_i = \sum_{k=1}^M a_{ik}, \quad a_j = \sum_{k=1}^M a_{kj}, \quad \bar{a}_i = \bar{a}_i = \frac{1}{n} a_i \quad (7)$$

$$a_{..} = \sum_{i,j=1}^M a_{ij}, \quad \bar{a} = \frac{1}{n^2} \sum_{i,j=1}^M a_{ij}, \quad (8)$$

$|X| = \langle X, X \rangle^{1/2}$  is the Euclidean norm and  $b_{ij}, \bar{b}_i, \bar{b}_j$  and  $\bar{b}$  are defined similarly for  $Y$ . It can be shown that this estimator for the distance correlation is unbiased with respect to  $q$  and  $p$ .

**GCL.** Consider an  $N \times M$  matrix  $X$  representing the gene expression of  $N$  genes from  $M$  single cells; that is, a matrix element  $x_{ij}$  represents the expression level of gene  $i$  in cell  $j$ . To quantify the GCL, we first divide the genes into two random subsets,  $S_1^*$  and  $S_2^*$ , and each of them consists of  $\frac{1}{2}N$  genes. Then, we measure the dependency level  $D^k = D_{\text{bcDecor}}(X_1, X_2)$  where  $X_1 = \{x_{ij}\}_{j \in S_1^*}$  and  $X_2 = \{x_{ij}\}_{j \in S_2^*}$ . In this study, we use the bcdCorr described above, but essentially any high-dimensional dependency measure can be used (for example, mutual information). We repeat these steps  $m$  times and define the GCL as the average of the dependency levels

$$\text{GCL}(X) \equiv \frac{1}{m} \sum_{k=1}^m D^k \quad (9)$$

In Extended Data Fig. 8, we show that the GCL stabilizes for  $m > 50$ . Accordingly, in our analysis we choose  $m = 50$ .

**Cell-to-cell variability.** Consider an  $N \times M$  matrix  $X$  representing the expression of  $N$  genes measured in  $M$  single cells, the cell-to-cell variability can be calculated for each gene separately or for the whole genome. The cell-to-cell variability gene  $i$  is given by  $\text{Var}(x_i) = \frac{1}{M} \sum_{j=1}^M (x_{ij} - \mu_i)^2$  where  $\mu_i = \frac{1}{M} \sum_{j=1}^M x_{ij}$  is the mean expression of gene  $i$  and  $x_{ij}$  represents the expression level of gene  $i$  in cell  $j$  (ref. <sup>9</sup>). For the whole genome, the cell-to-cell variability is given by  $\text{Var}(X) = \frac{1}{M} \sum_{j=1}^M (X_j - \mu)^2$  where  $\mu = \frac{1}{M} \sum_{j=1}^M X_j$  represents the expression profile on the 'average cell' and  $X_j$  represents the expression profile of cell  $j$  (ref. <sup>10</sup>).

**Modelling of GRNs.** We qualitatively demonstrate the GCL method on generated synthetic data, for eight different general models of GRNs. For all the models, the gene expression of an individual cell is set to be the steady state of coupled ordinary differential equations (ODEs), representing the dynamics of a set of genes with regulatory interactions<sup>25,38</sup>. The following eight ODEs represent the dynamics of the expression level of gene  $i$  for the different general models:

$$\frac{dx_i}{dt} = -B_i x_i + \sum_j w_{i,j}^{\text{act}} \frac{x_j}{1+x_j} \quad (10)$$

$$\frac{dx_i}{dt} = -B_i x_i + \sum_j w_{i,j}^{\text{rep}} \frac{1}{1+x_j} \quad (11)$$

$$\frac{dx_i}{dt} = -B_i x_i + \sum_j w_{i,j}^{\text{act}} \frac{x_j}{1+x_j} + \sum_j w_{i,j}^{\text{rep}} \frac{1}{1+x_j} \quad (12)$$

$$\frac{dx_i}{dt} = -B_i x_i + \sum_j w_{i,j}^{\text{act}} \frac{x_j}{1+x_j} + \sum_j w_{i,j}^{\text{rep}} \frac{1}{1+x_j} + \sum_{j,k} w_{i,j,k}^{\text{coop}} \frac{x_j}{1+x_j} \times \frac{x_k}{1+x_k} \quad (13)$$

$$\frac{dx_i}{dt} = -B_i x_i + \sum_j w_{i,j}^{\text{act}} \frac{x_j^2}{1+x_j^2} \quad (14)$$

$$\frac{dx_i}{dt} = -B_i x_i + \sum_j w_{i,j}^{\text{rep}} \frac{1}{1+x_j^2} \quad (15)$$

$$\frac{dx_i}{dt} = -B_i x_i + \sum_j w_{i,j}^{\text{act}} \frac{x_j^2}{1+x_j^2} + \sum_j w_{i,j}^{\text{rep}} \frac{1}{1+x_j^2} \quad (16)$$

$$\frac{dx_i}{dt} = -B_i x_i + \sum_j w_{i,j}^{\text{act}} \frac{x_j^2}{1+x_j^2} + \sum_j w_{i,j}^{\text{rep}} \frac{1}{1+x_j^2} + \sum_{j,k} w_{i,j,k}^{\text{coop}} \frac{x_j^2}{1+x_j^2} \times \frac{x_k^2}{1+x_k^2} \quad (17)$$

The first term in the right-hand side of each of the ODEs expresses a self (exponential) decay of gene  $x_i$  with degradation rate  $B_i$ . The other terms are input functions that capture the impact of all other genes on  $x_i$  through the GRN weighted interactions. Three input functions are used in our general models: the increasing Hill function  $w_{i,j}^{\text{act}} \frac{x_j^h}{1+x_j^h}$  for activation, the decreasing Hill function  $w_{i,j}^{\text{rep}} \frac{1}{1+x_j^h}$  for repression and multiplication of the two activation functions  $w_{i,j}^{\text{coop}} \frac{x_j^h}{1+x_j^h} \times \frac{x_k^h}{1+x_k^h}$  for cooperation<sup>25</sup>. In the first four ODEs, the Hill coefficient  $h$  is set to be 1 and for the other four  $h = 2$ .

In our simulations we set the degradation rate  $B_i$  to be 1, and for the active regulatory interactions (when the network  $w_{i,j} > 0$ ) the weights are randomly

chosen from a uniform distribution  $\mathbb{U}(0, 2)$ . In the models with only activation or repression, the networks, represented by  $w_{i,j}^{\text{act}}$  or  $w_{i,j}^{\text{rep}}$ , respectively, have an average degree  $k = 3$ . In the models that combine both activation and repression, the average degree of both networks  $w_{i,j}^{\text{act}}$  and  $w_{i,j}^{\text{rep}}$  is set at  $k = 1.5$  (so the total average degree is 3, as in the previous cases). In the models with activation, repression and cooperation, both networks  $w_{i,j}^{\text{act}}$  and  $w_{i,j}^{\text{rep}}$  have an average degree  $k = 1$  and in addition each gene  $x_i$  is regulated, on average, by two random coactivators genes ( $x_j$  and  $x_k$ ).

For a specific GRN model, defined by the set of  $w_{i,j}$ , the expression profile of a 'single cell' in a 'cohort' is generated by integrating the GRN differential equations with random initial conditions and evaluating the steady state using the ode45 MATLAB function. To simulate random damages in the GRNs of individual cells, for each cohort we first construct a 'base' GRN model defined by a set of parameters  $w_{i,j}^*$ . Then,  $M$  different GRN models are generated as random variations of this base model with the same network structure ( $w_{i,j}^{(\nu)} \neq 0$  wherever  $w_{i,j}^* \neq 0$ ,  $\nu = 1, \dots, M$ ) while the weights of the interactions are  $w_{i,j}^{(\nu)} = w_{i,j}^*$  with probability  $(1-p)$ , otherwise  $w_{i,j}^{(\nu)}$  are randomly chosen from a uniform distribution  $\mathbb{U}(0, 2)$ . In other words, all the  $M$  individual cells of the same cohort are generated from GRN models that share the same structure and weights of the base interaction matrix  $w^*$  while a fraction  $p$  of the weights are randomly changed. As  $p \rightarrow 0$  the model parameters become identical in all the GRN models of the same cohort. Thus,  $p$  quantifies the load of random errors in the dynamics of those models.

**Cell filtering procedure.** Gene expression is represented as the logarithm of the normalized counts, that is, transcript per million (TPM), for each cell,  $x_{ij} = \log_2(\text{TPM}_{ij} + 1)$ . We applied the same following process across all cell types and all the datasets: (1) remove genes that are expressed ( $x_{ij} > 2$ ) in less than 10% of the cells in each cohort, (2) filter cells for which the number of expressed genes ( $x_{ij} > 2$ ) is larger or smaller than two standard deviations from the mean number of expressed genes and (3) remove small clusters. We apply the  $k$ -means algorithm followed by Silhouette analysis that yields a score  $s_i$ , ( $i = 1, \dots, N$ ), for each cell and sum the scores  $S_{\text{kmeans}} = \sum_{i=1}^N s_i$ . We repeat the  $k$ -means and the Silhouette ten times and compare the realization with the maximal value of  $S_{\text{kmeans}}$  to the Silhouette analysis of a null model, where the cells are randomly assigned into groups of the same size as the  $k$ -means realization. We also apply t-SNE dimensional reduction visualization as a complementary analysis. We used these techniques to detect the presence of clusters in the data. If clusters are detected, we keep the largest cluster, detected using the  $k$ -means approach detailed above. (4) Calculate the Spearman distance between each cell and the mean cell and remove cells with a distance larger than two standard deviations above the average distance. (5) Calculate the Spearman distance between all pairs of cells and remove cells with distance smaller than four standard deviations below the average distance. (6) Finally, to further remove small clusters that were revealed only after the removal of outliers, we repeat the  $k$ -means approach over the PC1–PC2 plane from principal component analysis (PCA). See Supplementary Fig. 7 for a step by step example of the preprocess procedures.

**Removal of cycling cells.** For HSC cohorts, in addition to the standard preprocessing steps detailed above, to reduce technical noise in single-cell data created by cell division, we remove cells that were assigned a cell cycle phase other than 'G1' using the SCRN R package<sup>41</sup>. This phase was done before other filtering steps, to avoid erroneous assignment of the cell cycle phase<sup>42</sup>.

**Standard GCL analysis for all the datasets.** For each cohort of single cells, the GCL is calculated following these steps. (1) Select the intersection of two gene sets, each of them represents the top 5,000 highly expressed genes in young and old datasets separately. (2) Optionally, remove DEGs between young and old by calculating the two-tailed  $t$ -test with  $P < 0.05$ , adjusted for multiple comparisons by the Bonferroni procedure. (3) We perform bootstrap analysis by selecting 100 random subsets of genes with repeats, each subset consists 50% of the number of cells in the cohort, and calculate the GCL for each subset. Finally, the gene-to-gene coordination of each cohort is represented by a distribution of 100 GCL values.

**Pathway analysis. Preprocessing.** We analysed 330 pathways as annotated by KEGG<sup>32</sup>. The R programming language and the biomaRt package<sup>43,44</sup> are used to convert the gene identifiers to those used in the different analysed datasets. We applied the pathway analysis on LT-HSCs<sup>32,33</sup> and on MPP-HSCs<sup>32,39</sup>, on each dataset separately. We filter genes that are expressed ( $x_{ij} > 2$ ) in less than 20% of the cells of the cohort. Finally, we only analyse pathways that consist of at least 20 genes.

**Surrogate analysis.** We calculate the GCL of each pathway and compare it to the GCL values of 20 corresponding 'surrogate' gene sets, yielding a Z score for each pathway. The surrogate gene set are selected as follows: consider a set of  $n$  genes  $G = \{g_1, \dots, g_n\}$  that are annotated as a particular KEGG pathway. First, all  $N$  genes are ranked according to their mean expression, where  $k_i$  ( $i = 1, \dots, N$ ) represents the rank of gene  $i$ . Next, we choose a same-size surrogate gene set  $\tilde{G} = \{\tilde{g}_1, \dots, \tilde{g}_n\}$  such that for each gene  $g_i$  from the original pathway ( $g_i \in G$ ) we

randomly choose a gene  $\tilde{g}_j$  with the constraint that its expression rank  $k_{\tilde{g}_j}$  is similar to the rank  $k_g$  of original gene ( $k_g - 5 \geq k_{\tilde{g}_j} \geq (k_g + 5)$  and  $\tilde{g}_j \neq g_j$ ). The resulted surrogate gene set  $\tilde{G}$  preserves the size of the original pathway  $G$  and to mimic its expression profile but does not represent any known KEGG pathway. Finally, GCL<sub>surrogate</sub> values are calculated for 20 surrogate gene set  $\tilde{G}^{(v)}$  ( $v = 1, \dots, 20$ ). See schematic demonstration in Supplementary Fig. 3. We then calculate a Z score, defined as  $z \equiv \frac{(GCL_{pathway} - \text{mean}(GCL_{surrogate}))}{\text{std}(GCL_{surrogate})}$ .

**Cross-datasets pathway comparison of significantly elevated GCL.** When analysing the coordination of genes belonging to the same pathway, we found for each study a list of pathways with high Z score values. To test whether the three lists of pathways, extracted from the three different studies of HSCs, significantly overlap, we perform the following permutation test: (1) we first ‘label’ pathways with  $Z > 1$  as ‘high Z score’, in each study independently. The coordination of pathways in each study is then represented as a categorical variable. (2) We define a test statistic as the number of overlapping high Z score pathways, that is, the number of pathways that are labelled ‘high Z score’ in all three studies. (3) To test the dependence of the three categorical variables, we perform a permutation test. We shuffle the labels of the pathways in each study independently and calculate the test statistic. We repeat this step  $10^4$  times and obtain a distribution of the test statistic under the null hypothesis (independent variables). (4) Finally, we report one-tailed  $P$  values, calculated as the fraction of permutations with a number of overlap pathways equal or larger than the number in the original data. This analysis is shown in Extended Data Fig. 2j–k.

**GCL changes cross-datasets pathway analysis.** The pathways are classified into one of four categories in each of three datasets independently, and then are qualitatively compared across the different datasets. For the classification we consider three values for each pathway: the Z score calculated for young cells,  $Z$  score<sub>young</sub>, comparing between the pathway and surrogate gene sets (as detailed above), the Z score calculated for old cells,  $Z$  score<sub>old</sub>, and a direct comparison between the GCL values of young and old cells  $\Delta_{GCL} = \frac{\text{mean}(GCL_{old}) - \text{mean}(GCL_{young})}{\text{std}(GCL_{old}) + \text{std}(GCL_{young})}$ . A pathway is classified as ‘decreased GCL’ if (1) its  $Z$  score<sub>young</sub>  $> 1$  and (2) either the  $Z$  score<sub>old</sub>  $< 1$  or  $\Delta_{GCL} < (-1)$ . Similarly, A pathway is classified as ‘increased GCL’ if (1) its  $Z$  score<sub>old</sub>  $> 1$  and (2) either the  $Z$  score<sub>young</sub>  $< 1$  or  $\Delta_{GCL} > 1$ . If, however,  $Z > 1$  in both young and old cells, and  $|\Delta_{GCL}| < 1$ , the pathway is classified as ‘unchanged’. Otherwise, if a pathway does not meet the definitions of the previous categorizations, it is classified as ‘insignificant’. Finally, we consider a ‘validated’ classification of Increased GCL or ‘decreased GCL’ of a pathway if there is an agreement across three independent studies, or across two studies and the third one is either ‘unchanged’ or ‘insignificant’. Unvalidated pathways are considered ‘disputed’ pathways.

To evaluate the statistical significance of the validated classifications, that is, whether the validated pathways represent characteristic features that are preserved across studies, we compare the number of pathways in each category to the number under a null model of no correlation between the studies. In the null model, we shuffle the classifications of the pathways in each study and repeat the cross-validation procedure described above to evaluate the chance for accidental ‘agreement’ between studies. We then compare the number of validated pathways in the real data to the number in the shuffled data. We report one-tailed  $P$  values for each category, calculated as the fraction of null-model realizations with several pathways equal or larger than the number in the original data.

**Dataset analysis.** In this study we analyse more than 20 cohorts of cells representing very different species (fruit fly, mouse and human) and very different cell types (HSCs, immune cells, pancreatic cells, neurons and glial cells). Table 1 includes the information of the organism (mice strain where relevant), tissue type, cell type, number of cells, ages and sex.

**Reporting Summary.** Further information on research design is available in the Nature Research Reporting Summary linked to this article.

## Data availability

All datasets analysed in this study are publicly available as described in Table 1, and the accession codes and references are provided in Supplementary Table 1.

## Code availability

The custom MATLAB code for computing the GCL that was used in this study is available at <https://github.com/guy531/gcl/blob/master/gcl.m>.

Received: 16 April 2020; Accepted: 22 September 2020;

Published online: 02 November 2020

## References

- Moskalev, A. A. The role of DNA damage and repair in aging through the prism of Koch-like criteria. *Ageing Res. Rev.* **12**, 661–684 (2013).
- Benayoun, B. A., Pollina, E. A. & Brunet, A. Epigenetic regulation of ageing: linking environmental inputs to genomic stability. *Nat. Rev. Mol. Cell Biol.* **16**, 593–610 (2015).
- Kirkwood, T. B. L. Understanding the odd science of aging. *Cell* **120**, 437–447 (2005).
- Aubert, G. & Lansdorp, P. M. Telomeres and aging. *Physiol. Rev.* **88**, 557–579 (2008).
- McHugh, D. & Gil, J. Senescence and aging: causes, consequences, and therapeutic avenues. *J. Cell Biol.* **217**, 65–77 (2018).
- van Deursen, J. M. Senolytic therapies for healthy longevity. *Science* **364**, 636–637 (2019).
- Vijg, J. Impact of genome instability on transcription regulation of aging and senescence. *Mech. Ageing Dev.* **125**, 747–753 (2004).
- López-Otín, C., Blasco, M. A., Partridge, L., Serrano, M. & Kroemer, G. The hallmarks of aging. *Cell* **153**, 1194–1217 (2013).
- Booth, L. N. & Brunet, A. The aging epigenome. *Mol. Cell* **62**, 728–744 (2016).
- Gems, D. & Partridge, L. Genetics of longevity in model organisms: debates and paradigm shifts. *Annu. Rev. Physiol.* **75**, 621–644 (2013).
- Vijg, J. & Dong, X. Pathogenic mechanisms of somatic mutation and genome mosaicism in aging. *Cell* **182**, 12–23 (2020).
- Levsky, J. M. & Singer, R. H. Gene expression and the myth of the average cell. *Trends Cell Biol.* **13**, 4–6 (2003).
- Bahar, R. et al. Increased cell-to-cell variation in gene expression in ageing mouse heart. *Nature* **441**, 1011–1014 (2006).
- Busuttil, R., Bahar, R. & Vijg, J. Genome dynamics and transcriptional deregulation in aging. *Neuroscience* **145**, 1341–1347 (2007).
- Martinez-Jimenez, C. P. et al. Aging increases cell-to-cell transcriptional variability upon immune stimulation. *Science* **355**, 1433–1436 (2017).
- Enge, M. et al. Single-cell analysis of human pancreas reveals transcriptional signature of aging and somatic mutation patterns. *Cell* **171**, 321–330.e14 (2017).
- Ilias, A. et al. An atlas of the aging lung mapped by single cell transcriptomics and deep tissue proteomics. *Nat. Commun.* **10**, 963 (2019).
- Wang, J. et al. A differentiation checkpoint limits hematopoietic stem cell self-renewal in response to DNA damage. *Cell* **148**, 1001–1014 (2012).
- Rossi, D. J. et al. Deficiencies in DNA damage repair limit the function of hematopoietic stem cells with age. *Nature* **447**, 725–729 (2007).
- Rossi, D. J. et al. Hematopoietic stem cell quiescence attenuates DNA damage response and permits DNA damage accumulation during aging. *Cell Cycle* **6**, 2371–2376 (2007).
- Rossi, J. et al. Stem cells and the pathways to aging and cancer. *Cell* **132**, 681–696 (2008).
- Warren, L. A. et al. Transcriptional instability is not a universal attribute of aging. *Aging Cell* **6**, 775–782 (2007).
- Zhang, Q. et al. Systems-level analysis of human aging genes shed new light on mechanisms of aging. *Hum. Mol. Genet.* **25**, 2934–2947 (2016).
- Southworth, LucindaK., Art, B., Owen & Stuart, K. Kim Aging mice show a decreasing correlation of gene expression within genetic modules. *PLoS Genet.* **5**, e1000776 (2009).
- Alon, U. *An Introduction to Systems Biology: Design Principles of Biological Circuits* (Chapman and Hall/CRC, 2006).
- McNabb, D. S., Xing, Y. & Guarente, L. Cloning of yeast HAP5: a novel subunit of a heterotrimeric complex required for CCAAT binding. *Genes Dev.* **9**, 47–58 (1995).
- Davidson, E. H. et al. A genomic regulatory network for development. *Science* **295**, 1669–1678 (2002).
- Shen-Orr, S., Milo, R., Mangan, S. & Alon, U. Network motifs in the transcriptional regulation network of *Escherichia coli*. *Nat. Genet.* **31**, 64–68 (2002).
- Buchler, N. E., Gerland, U. & Hwa, T. On schemes of combinatorial transcription logic. *Proc. Natl Acad. Sci. USA* **100**, 5136–5141 (2003).
- Székely, G. J. & Rizzo, M. L. The distance correlation  $t$ -test of the independence in high dimension. *J. Multivar. Anal.* **117**, 193–213 (2013).
- Mann, M. et al. Heterogeneous responses of hematopoietic stem cells to inflammatory stimuli are altered with age. *Cell Rep.* **25**, 2992–3005 (2018).
- Ogata, H. et al. KEGG: Kyoto Encyclopedia of Genes and Genomes. *Nucleic Acids Res.* **27**, 29–34 (1999).
- Kowalczyk, M. S. et al. Single-cell RNA-seq reveals changes in cell cycle and differentiation programs upon aging of hematopoietic stem cells. *Genome Res.* **25**, 1860–1872 (2015).
- Grover, A. et al. Single-cell RNA sequencing reveals molecular and functional platelet bias of aged haematopoietic stem cells. *Nat. Commun.* **7**, 11075 (2016).
- Yang, L. et al. Single-cell RNA-seq of esophageal squamous cell carcinoma cell line with fractionated irradiation reveals radioresistant gene expression patterns. *BMC Genomics* **20**, 611 (2019).
- Kelley, R. in *Systems Biology in Practice: Concepts, Implementation, and Application* (eds Klipp, E. et al.) (Wiley-Blackwell, 2005).
- Ackers, G. et al. Quantitative model for gene regulation by lambda phage repressor. *Proc. Natl Acad. Sci. USA* **79**, 1129 (1982).

38. Karlebach, G. & Shamir, R. Modelling and analysis of gene regulatory networks. *Nat. Rev. Mol. Cell Biol.* **9**, 770–780 (2008).
39. Steelman, L. S. et al. Roles of the Raf/MEK/ERK and PI3K/PTEN/Akt/mTOR pathways in controlling growth and sensitivity to therapy—implications for cancer and aging. *Aging* **3**, 192–222 (2011).
40. Székely, G. J., Rizzo, M. L. & Bakirov, N. K. Measuring and testing dependence by correlation of distances. *Ann. Stat.* **35**, 2769–2794 (2007).
41. Lun, A. T. L., McCarthy, D. J. & Marioni, J. C. A step-by-step workflow for low-level analysis of single-cell RNA-seq data with Bioconductor. *F1000 Res.* **5**, 2122 (2016).
42. Scialdon, A. et al. Computational assignment of cell-cycle stage from single-cell transcriptome data. *Methods* **85**, 54–61 (2015).
43. Durinck, S. et al. BioMart and Bioconductor: a powerful link between biological databases and microarray data analysis. *Bioinformatics* **21**, 3439–3440 (2005).
44. Durinck, S., Spellman, P. T. & Huber, W. Mapping identifiers for the integration of genomic datasets with the R/Bioconductor package biomaRt. *Nat. Protoc.* **4**, 1184–1191 (2009).
45. Davie, K. et al. A single-cell transcriptome atlas of the aging *Drosophila* brain. *Cell* **174**, 982–998.e20 (2018).
46. Young, K. et al. Progressive alterations in multipotent hematopoietic progenitors underlie lymphoid cell loss in aging. *J. Exp. Med.* **213**, 2259–2267 (2016).

## Acknowledgements

We thank M. Enge for sharing experimental data and for his helpful support. We also thank M.L. Rizzo, E. Eisenberg, Y. Brody, R. Cohen and S. Havlin for helpful discussions. Y.-Y.L. acknowledged grants from National Institutes of Health (R01AI141529, R01HD093761, UH3OD023268, U19AI095219 and U01HL089856). The project

described was supported in part by award numbers R01 HL124233 and R01 HL147326 from the National Heart, Lung, and Blood Institute and the FDA Center for Tobacco Products (CTP). The content is solely the responsibility of the authors and does not necessarily represent the official views of the NIH or the Food and Drug Administration. A.B. thanks the Azrieli Foundation for supporting this research.

## Author contributions

A.B., O.L. and G.A. conceived and designed the project. O.L. and G.A. performed real data analysis, D.V. performed the simulations. T.S. performed the bioinformatics analysis of pathways. A.B., O.L., G.A., D.V., T.S., S.E., P.C., Y.-Y.L. and H.Y.C. analysed the results. A.B., O.L. and G.A. wrote the manuscript with contributions from all authors.

## Competing interests

The authors declare no competing interests.

## Additional information

**Extended data** is available for this paper at <https://doi.org/10.1038/s42255-020-00304-4>.

**Supplementary information** is available for this paper at <https://doi.org/10.1038/s42255-020-00304-4>.

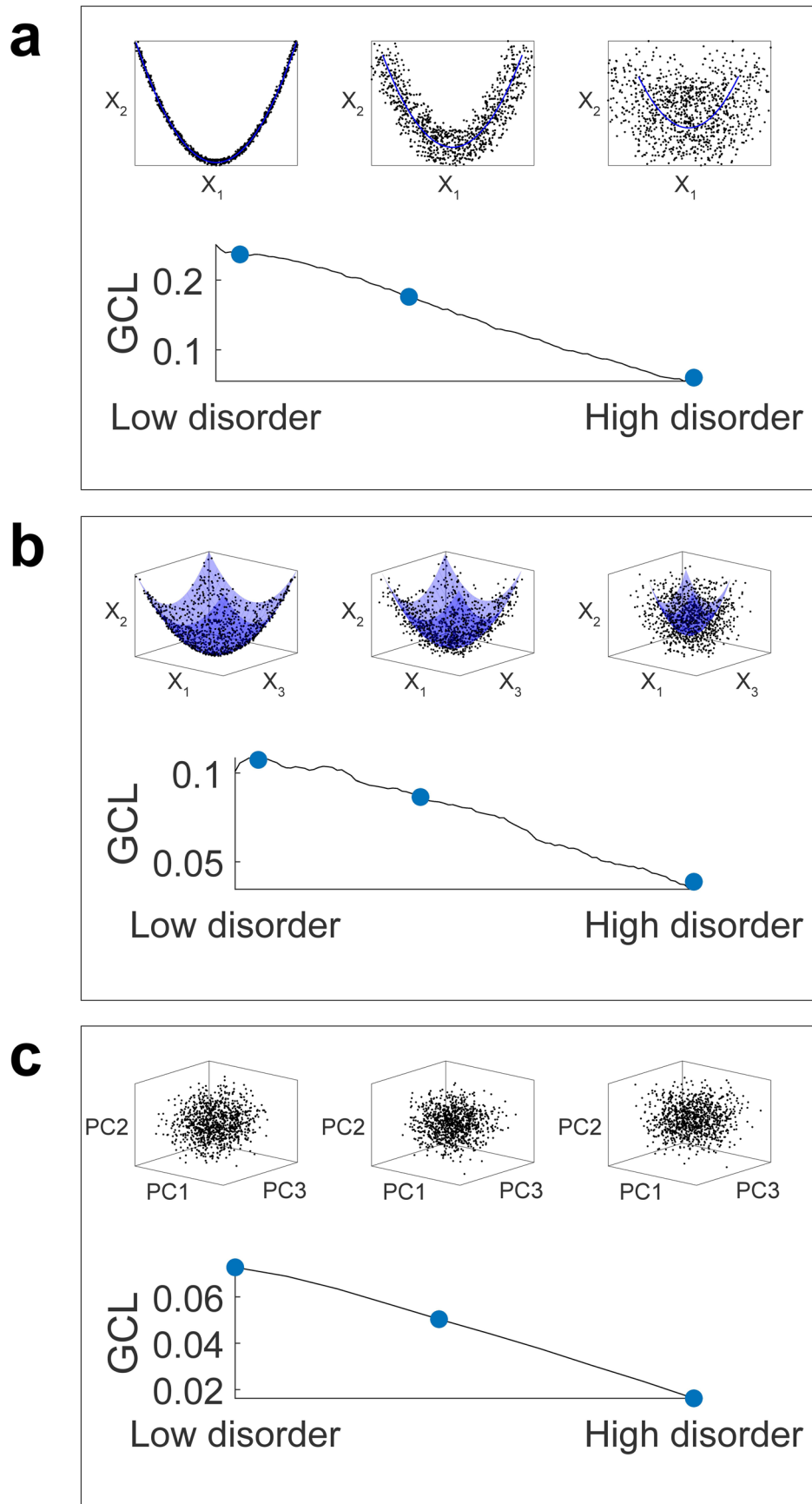
**Correspondence and requests for materials** should be addressed to A.B.

**Peer review information** Primary Handling Editor: Pooja Jha.

**Reprints and permissions information** is available at [www.nature.com/reprints](http://www.nature.com/reprints).

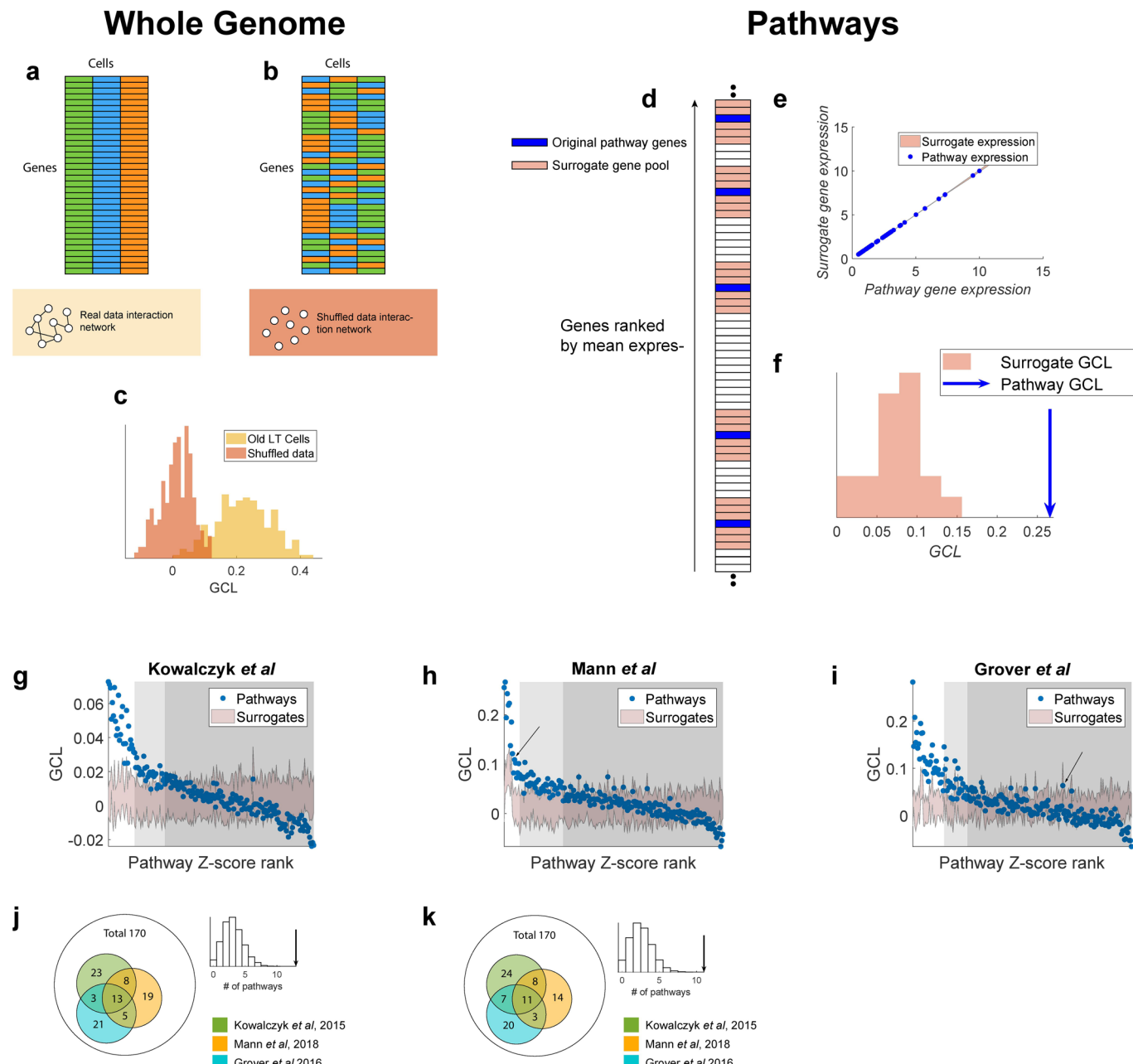
**Publisher's note** Springer Nature remains neutral with regard to jurisdictional claims in published maps and institutional affiliations.

© The Author(s), under exclusive licence to Springer Nature Limited 2020

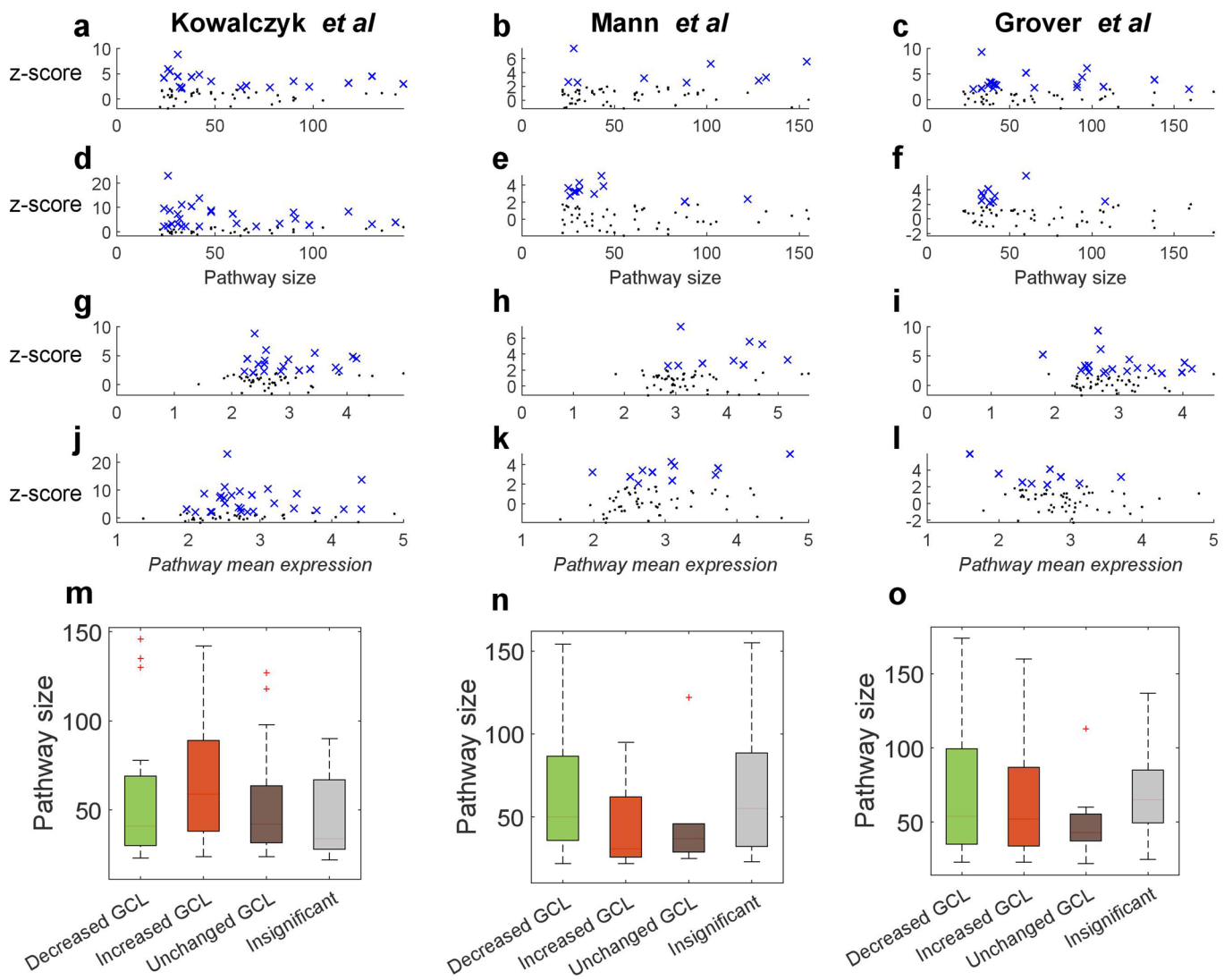


Extended Data Fig. 1 | See next page for caption.

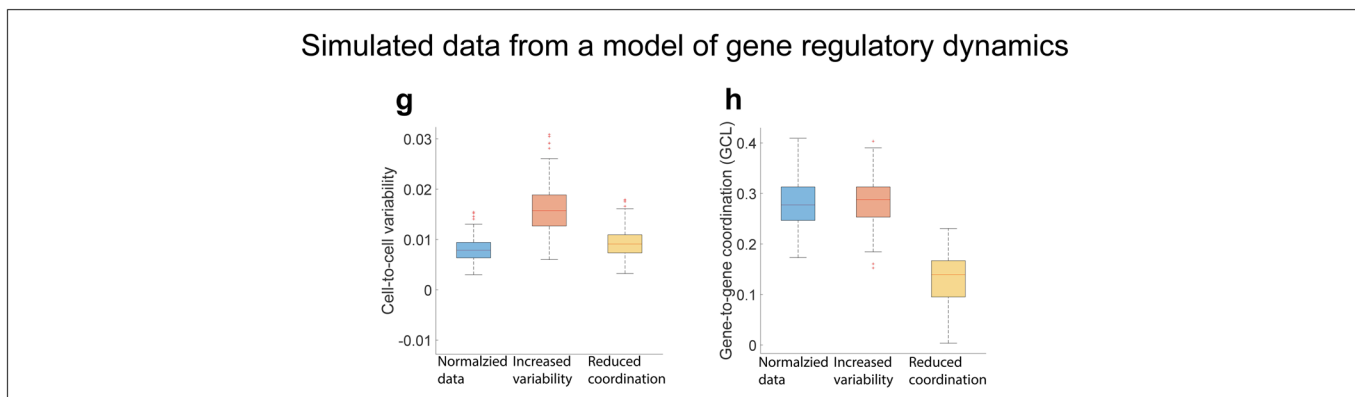
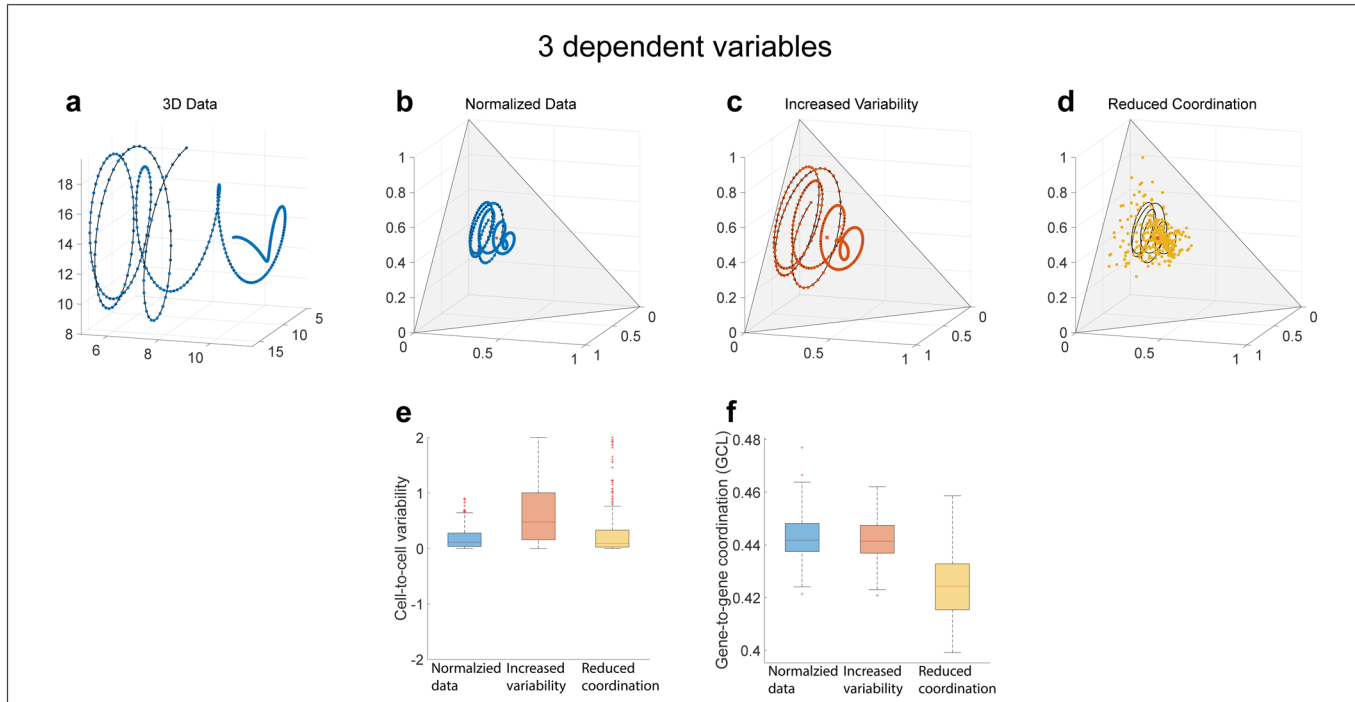
**Extended Data Fig. 1 | Illustration of global coordination level (GCL) for high-dimensional dependency analysis.** **a**, An example of a simple dependency form between two variables is given by  $x_2 = x_1^2$ . The possible states are represented as points over the  $x_1$ - $x_2$  plane, where a disorder (random variable from a uniform distribution) is then added into each variable independently. For low disorder levels, the points lie on or very close to the 1D manifold (blue curve). As the disorder amplitude increases, the points lie farther from the manifold. For high disorder levels, the relationship between the variables is virtually indistinguishable from random noise, and the points fill the 2D embedding space. Correspondingly, the GCL decreases as the disorder level increases. The three blue circles represent the GCL values calculated for the three examples above. Note that the absolute GCL values are dependency-form-specific and are used to compare between entities. **b**, Similar to a for three variables, with a dependency given by  $x_3 = x_1^2 + x_2^2$ , while a disorder term is then added into each variable independently. For low disorder the points lie on a 2D manifold, while for high disorder the points are farther from the manifold and fill the 3D embedding space. **c**, Like a and b but for ten variables. The dependency is given by  $x_N = \sum_{i=1}^{N-1} x_i^2$  with  $N=10$ . In this case, the lower-dimensional manifold cannot be represented even after applying the standard dimensional reduction technique (PCA). Thus, the three cases of different disorder levels look similar in the reduced space. However, the differences are captured by the GCL analysis.



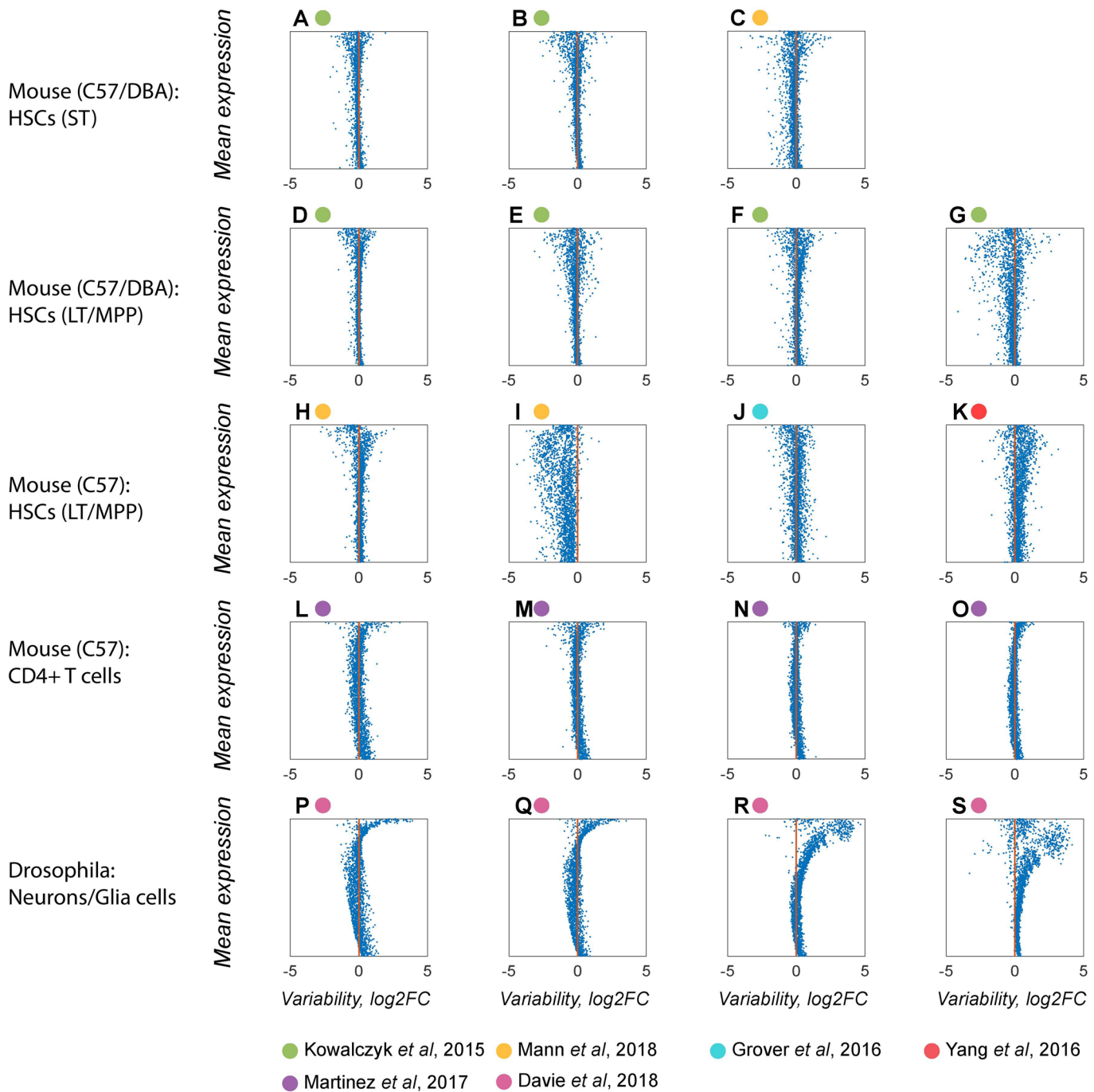
**Extended Data Fig. 2 | GCL captures effect of gene-to-gene dependency and functional relations.** **(a, b)** Schematic demonstration of the shuffling procedure. **a**, Gene expression of three individual cells are represented by different colors. **b**, Shuffled data across different cells, preserving the statistical properties of the individual genes, whilst removing the effects of the relationships between the genes, if any exists. **c**, GCL values of real data (yellow histogram) compared with shuffled data (red histogram). Since the effects of interrelations between the gene are effectively lost in the shuffled data, the GCL values are centered around zero. While are significantly higher in the real data. **d**, Visualization of the surrogate preparing process. Each pathway is composed of several genes with different mean expression values. We sort the genes by their mean expression values and for each gene belonging to the pathway (blue) we identify a subset of genes with similar expression values (pink). A surrogate expression profile is generated by selecting a random gene from each subset. This allows us to generate many surrogate pathways with similar expression values. **e**, The expression levels of the 'T cell receptor signalling pathway' are shown versus the mean values of the corresponding surrogate gene sets ( $n=20$ ). The red area represents the range of expression values of the surrogate gene sets, demonstrating their similarity to the real pathway. **f**, GCL values of the real pathway (blue arrow) and the surrogate pathways (red histogram). Even though the expression profiles are very similar, the GCL of the real pathway is significantly higher than the surrogate pathway ( $P<0.05$ ). This suggests that higher coordination is associated with real biological function. **g, h, i**, GCL values of pathways are compared with GCL values of compatible surrogate gene-sets, yielding a Z-score, by which the pathways are sorted in the figure. White, light-grey and dark-grey backgrounds mark pathways with  $Z\text{-score}>2$ ,  $1<Z\text{-score}<2$  and  $Z\text{-score}<1$ , respectively. **j**, The lists of 'high Z-score' pathways ( $Z\text{-score}>1$ ) in young LT-HSCs are compared across the three studies (colored areas in Venn diagrams). The number of pathways labeled as 'high Z-score' in all three datasets (marked with an arrow in the inset) is significantly higher compared with random permutations of the labeled pathways (see Methods section) ( $P<10^{-4}$ ). **k**, Same as **j** but for old cells ( $P<10^{-4}$ ). The total number of analyzed pathways is 170.



**Extended Data Fig. 3 | Pathways Z-score as a function of mean gene expression.** GCL values of pathways are compared with GCL values of matching surrogate gene-sets, yielding a Z-score for each KEGG pathway. In addition, for each pathway with a set of  $n$  annotated genes, we calculate the mean expression of the log-transformed TPMs, that is,  $\frac{1}{n} \sum_{j \in G} \log_2(\text{TPM}_{i,j} + 1)$ . Each pathway is represented as a point. **a**, young cells from Ref. <sup>33</sup>; **b**, young cells from Ref. <sup>31</sup>; **c**, young cells from Ref. <sup>34</sup>; **d**, old cells from Ref. <sup>33</sup>; **e**, old cells from Ref. <sup>31</sup>; **f**, old cells from Ref. <sup>34</sup>. Pathways with  $z\text{-score} > 2$  are marked with an X symbol. **g-l**, like **a-f** but for mean expression value. In all datasets we do not observe a correlation between the Z-score and the mean expression level or pathway size. **m-o**, Pathway size distribution by group association of aging (see Fig. 4). A two-tailed, unpaired t-test with unequal variances showed no significant differences between any group pathway size distribution (all  $p$ -values are larger than 0.1). We conclude therefore that there is no correlation between pathway size and aging effects of GCL on the pathways.

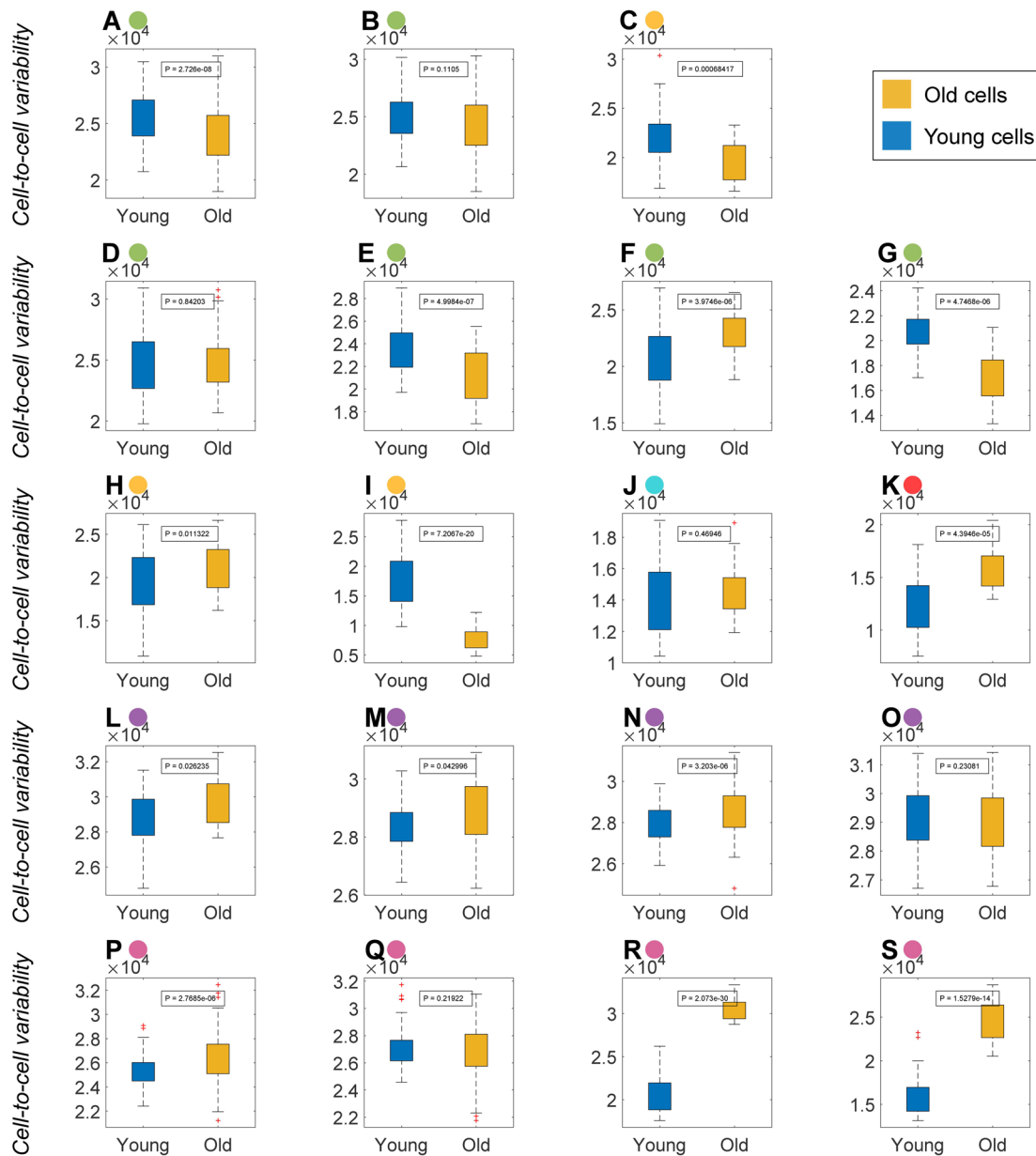


**Extended Data Fig. 4 | Cell-to-cell variability and Gene-to-gene coordination are independent measures.** We show here two examples of how cell-to-cell variability and gene-to-gene coordination (GCL) can be independently changed on simulated data. On the top box we analyze data of 3 dependent variables. **a**, The dependency between the three variables is shown (black line) along with 1000 simulated samples on it (blue dots). **b**, The data is shown on the 2-simplex after normalization along with the mean sample, indicated by the red cross sign. **c**, A manipulation on the data which increases the variability but does not affect the GCL value. Each point is stretched away from the mean point with a fixed distance whilst keeping all the samples normalized. This causes the variability to increase (since each point is further away from the mean point), but the variables are still completely dependent which ensures the GCL does not change. **d**, A manipulation on the data which decreases the GCL but does not affect the variability. Each point is moved towards or away from the mean point randomly. This does not affect the total distance from the mean point (which is the variability) but does break the dependency between the variables causing the GCL to decrease. **e**, and **f**, The variability and GCL of the three cases above, color coded according to the cases. It is clear that the variability and GCL can be independently manipulated. The variability was calculated using Euclidean distance of each point from the mean on the normalized space and the GCL was calculated using bootstrap method with 200 samples per bootstrap and 100 bootstraps. Bottom box, **g** and **h**: We show a similar analysis on simulated data based on Michaelis-Menten simulations of 400 genes and 200 samples (see Methods sec., *Modelling of Gene Regulatory Networks*). The GCL was calculated with bootstrap method, using 50 random cuts, 50 samples per bootstrap and 100 bootstraps. Here again it is clear that the two measures are independent from each other and are indicative of completely different properties of the data. Center line, median; box limits, upper and lower quartiles; whiskers, 1.5x interquartile range; points, outliers.



**Extended Data Fig. 5 | Systematic analysis of cell-to-cell variability (1).** The cell-to-cell variability of each of the cohorts in Fig. 2 is evaluated using the measure presented by Ref. 15. Each point represents the change of variability in aging defined as  $\log_2 \frac{\text{var}(\text{old})}{\text{var}(\text{young})}$ , where 'var(young)' and 'var(old)' represent the variance of a single gene in young and in old cells, respectively ST-HSCs from C57BL/6 mice (a) and DBA/2 mice (b) from Ref. 33 (c) from Ref. 31. LT-HSCs from C57BL/6 mice (d) and DBA/2 mice (e), MPP-HSCs from C57BL/6 mice (f) and DBA/2 mice (g) from Ref. 33, LT-HSCs (h) and MPP-HSCs (i) from C57BL/6 mice from Ref. 31, LT-HSCs from C57BL/6 mice from Ref. 34 (j) and MPP-HSCs from C57BL/6 mice from Ref. 46 (k), mouse immune CD4+ T cells, stimulated effector memory cells (l), stimulated naïve cells (m), unstimulated naïve cells (n) and unstimulated effector memory cells (o) from Ref. 15, *Drosophila melanogaster* Glia cells - 'Astrocyte-like' (p), 'Ensheathing' (q) and *Drosophila* neurons - neurons of the optic lobes ('Dm8.Tm5c') (r) and antero-dorsal olfactory projection neurons ('OPN.adPNandPN') (s) from Ref. 45. There is no clear tendency of increased variability upon aging.

Mouse (C57/DBA):  
HSCs (ST)



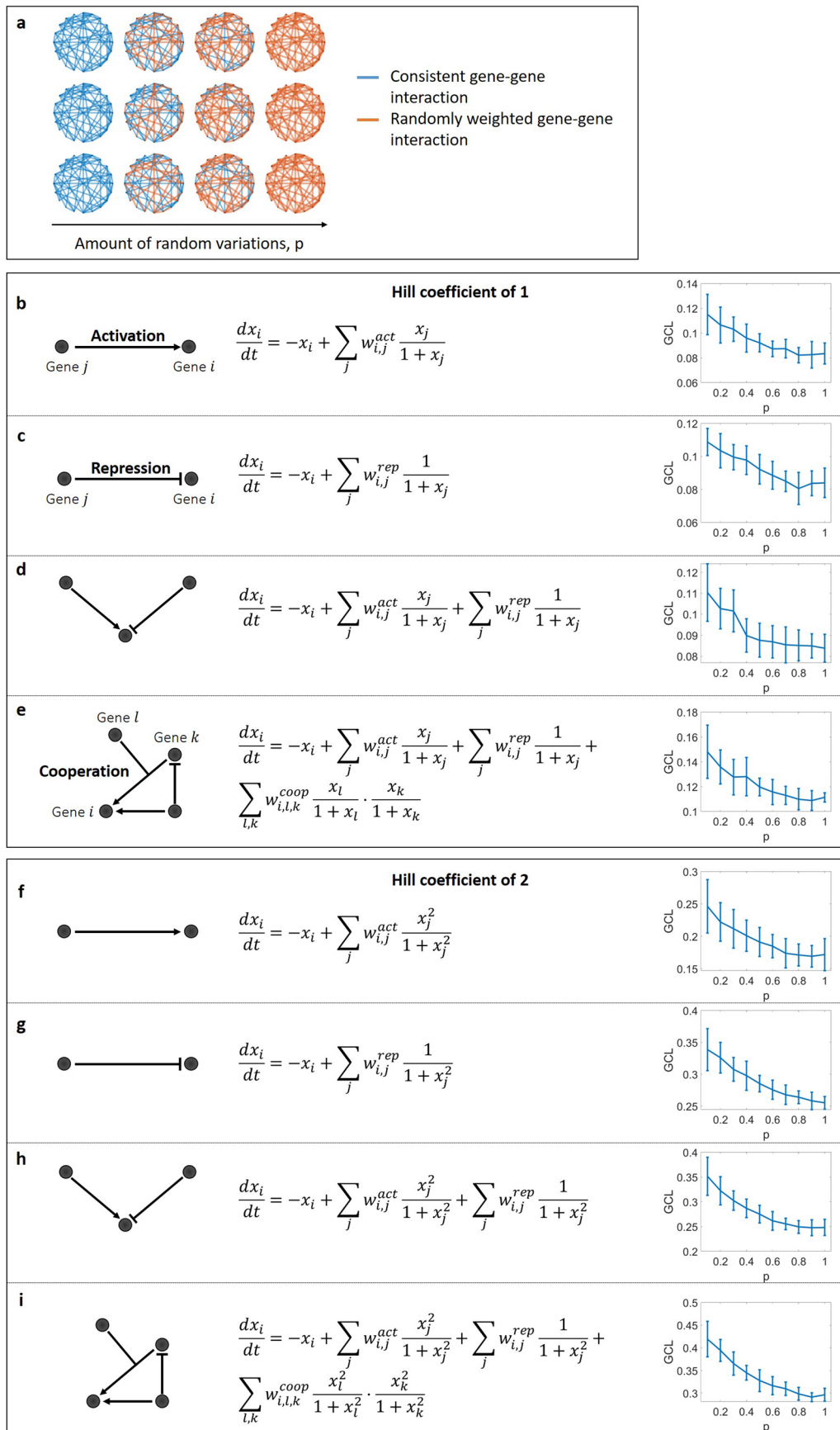
● Kowalczyk et al., 2015   ● Mann et al., 2018

● Martinez et al., 2017   ● Davie et al., 2018

● Grover et al., 2016

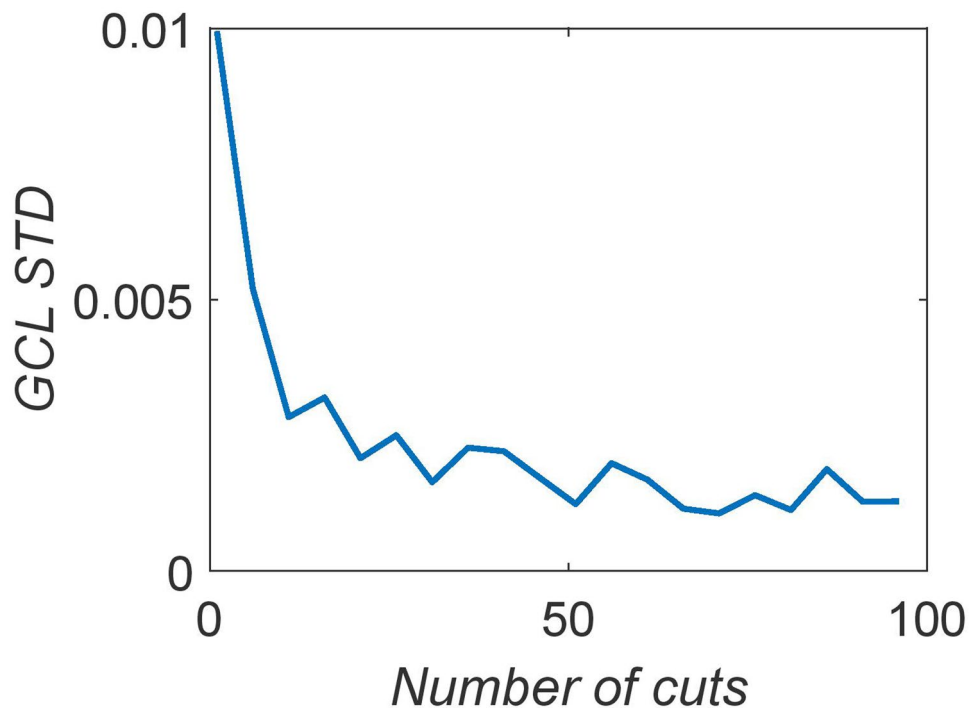
● Yang et al., 2016

**Extended Data Fig. 6 | Systematic analysis of cell-to-cell variability (2).** The cell-to-cell variability of each of the cohorts in Fig. 2 is evaluated using the measure presented by Ref. 16. ST-HSCs from C57BL/6 mice (a) and DBA/2 mice (b) from Ref. 33 (c) from Ref. 31. LT-HSCs from C57BL/6 mice (d) and DBA/2 mice (e), MPP-HSCs from C57BL/6 mice (f) and DBA/2 mice (g) from Ref. 33, LT-HSCs (h) and MPP-HSCs (i) from C57BL/6 mice from Ref. 31, LT-HSCs from C57BL/6 mice from Ref. 34 (j) and MPP-HSCs from C57BL/6 mice from Ref. 46 (k), mouse immune CD4+ T cells, stimulated effector memory cells (l), stimulated naïve cells (m), unstimulated naïve cells (n) and unstimulated effector memory cells (o) from Ref. 15, *Drosophila melanogaster* Glia cells -, 'Astrocyte-like' (p), 'Ensheathing' (q) and Drosophila neurons - neurons of the optic lobes ('Dm8.Tm5c') (r) and antero-dorsal olfactory projection neurons ('OPN.adPNandPN') (s) from Ref. 45. There is no clear tendency of increased variability upon aging. Center line, median; box limits, upper and lower quartiles; whiskers, 1.5x interquartile range; points, outliers. \*,  $P < 10^{-10}$  using two-tailed, unpaired, unequal variance t-test; NS,  $P > 10^{-3}$ , adjusted for multiple comparisons by the Bonferroni procedure. The number of cells in each group is reported in Extended Data Table 1.



Extended Data Fig. 7 | See next page for caption.

**Extended Data Fig. 7 | GCL decrease with damages accumulation in simulations of gene regulatory networks.** Synthetic gene-expression profiles were calculated for eight different generic mathematical models of gene regulatory networks (GRNs). For each generic model we generated cohorts of 200 cell profiles of 400 genes, where each cohort has a ‘base’ GRN dynamics. The expression profile of a cell in a cohort is set to be the steady state of an individual GRN model, which is produced by randomly changing  $p$  fraction of the base’s GRN weights (see Methods Sec.). **a**, Illustration of three individual models of regulatory networks with four different values of  $p$  (from left to right: 0, 0.33, 0.67, 1). Nodes represent genes and links represent regulatory interactions. In the left column ( $p=0$ ) all three individual models have the same dynamics, represented by the blue links. As  $p$  increases, the weight of each interaction is randomly reassigned with probability  $p$ , in each model independently, represented by an orange link, leading to increased heterogeneity. **b–i**, Simulations were performed for eight different mathematical models of gene regulation: **b**, Only activating transcriptional regulations with Hill coefficient of 1. **c**, Only repression transcriptional regulations with Hill coefficient of 1. **d**, Both activation and repression with Hill coefficient of 1. **e**, Activation + repression + cooperativity of two co-activators with Hill coefficient of 1. **f–i**, same as **b–e** but with Hill coefficient of 2. For each model, the dynamics of each gene is represented by an ordinary differential rate equation. The GCL was calculated with the bootstrap method, using 20 random cuts. Data points and error bars represent mean and standard deviation over 5 realizations, respectively.



**Extended Data Fig. 8 | Standard deviation of GCL as a function of the number of division (M).** Analysis was done for young LTHSC from Ref. <sup>12</sup> with 113 cells and 2000 genes. We perform bootstrap analysis where each bootstrap realization had a random subset of 80% of the cells. The GCL STD is the standard deviations of the GCL calculated for each bootstrap (with 20 bootstrap realizations in total). The GCL STD stabilizes around 50 divisions. For analysis of the whole genome of the rest of the datasets we chose 50 divisions as well.